White Rose Research Online

eprints@whiterose.ac.uk
https://eprints.whiterose.ac.uk
Universities of Leeds, Sheffield and York

Deposited via The University of Leeds.

White Rose Research Online URL for this paper:
https://eprints.whiterose.ac.uk/id/eprint/242906/

Version: Accepted Version

Article:
Nimaming, N., Sadeghpour, A., Murray, B.S. et al. (2026) Interfacial properties of plant protein–flavonoid hybrid particles: towards influencing in vitro gastric digestion of emulsions. Food Chemistry, 525 (Part 1). 150307. ISSN: 0308-8146

https://doi.org/10.1016/j.foodchem.2026.150307

This is an author produced version of an article published in Food Chemistry, made available via the University of Leeds Research Outputs Policy under the terms of the Creative Commons Attribution License (CC-BY), which permits unrestricted use, distribution and reproduction in any medium, provided the original work is properly cited.

Reuse
This article is distributed under the terms of the Creative Commons Attribution (CC BY) licence. This licence allows you to distribute, remix, tweak, and build upon the work, even commercially, as long as you credit the authors for the original work. More information and the full terms of the licence here: https://creativecommons.org/licenses/

Takedown
If you consider content in White Rose Research Online to be in breach of UK law, please notify us by emailing eprints@whiterose.ac.uk including the URL of the record and the reason for the withdrawal request.

UNIVERSITY OF LEEDS
University of Sheffield
UNIVERSITY of York

Interfacial properties of plant protein–flavonoid hybrid particles: Towards influencing *in vitro* gastric digestion of emulsions

Nisufyan Nimaming[1, 2], Amin Sadeghpour[1], Brent S. Murray[1, 3], Anwesha Sarkar[1, 3]*

[1]*Food Colloids and Bioprocessing Group, School of Food Science and Nutrition, University of Leeds, Leeds, LS2 9JT, United Kingdom.*

[2]*Food and Nutrition, Faculty of Home Economics Technology, Rajamangala University of Technology Krungthep, Bangkok, 10120, Thailand*

[3]*National Alternative Protein Innovation Centre (NAPIC), UK*

Corresponding author:

*Prof. Anwesha Sarkar

[1] Food Colloids and Bioprocessing Group, School of Food Science and Nutrition, University of Leeds, Leeds LS2 9JT, UK.

[3] National Alternative Protein Innovation Centre (NAPIC), UK

E-mail address: A.Sarkar@leeds.ac.uk

Highlights

- The hybrid particles (PoPQC) shows minimal pH-dependent changes in size
- In low pH, PoPQC yields more viscoelastic films than non-hybrid counterparts
- High ionic strengths markedly strengthen PoPQC interfacial films
- PoPQC-stabilised emulsions are resistant to proteolysis during gastric digestion
- PoPQC at the interface prevents droplet coalescence during gastric digestion

Abstract

This study evaluated the interfacial performance of potato protein-quercetin hybrid particles (PoPQC) at oil-water interfaces and how such hybrid particle-laden interface provides stability to Pickering emulsions droplets during *in vitro* gastric digestion. Dynamic adsorption and interfacial shear rheology of PoPQC dispersions as a function of pH 3.0–9.0 and 100–250 mM NaCl (pH 7.0) and the microstructural evolution of the emulsions stabilized by these plant protein-hybrid particles were examined under *in vitro* gastric digestion. Remarkably, PoPQC dispersions exhibited limited pH-dependent size changes, showing resistance to isoelectric precipitation unlike the non-hybrid potato protein (PoP). Complexation with QC reduced hydrophobic PoP–PoP interaction and promoted the formation of elastic interfacial layers which strengthened with increased ionic strengths. The robustness of the PoPQC interfacial structure offered microstructural stability to the emulsified lipids unlike those emulsions stabilized by PoP in the gastric phase, highlighting the potential of hybrid particles for controlling gastric coalescence.

Keywords: potato protein; quercetin; interfacial shear rheology; Pickering emulsion; alternative protein; interfacial tension

1. Introduction

Plant proteins either alone or in combination with other natural materials are increasingly becoming common in various food emulsions as emulsifiers for making sustainable food formulations (Nimaming, Sadeghpour, Murray, & Sarkar, 2024; Sarkar & Dickinson, 2020). Proteins play an important role in the stabilization of emulsions and foams (Sarkar & Singh, 2016). Proteins adsorb strongly at oil–water (O–W) and air–water (A–W) interfaces owing to their mixed hydrophilic/hydrophobic nature and their ability to self-assemble into two-dimensional viscoelastic layers upon adsorption (Bergfreund, Bertsch, & Fischer, 2021a; Bergfreund et al., 2021b; Dickinson, 1999) that enhances the corresponding colloidal stability (Murray, 2002, 2011; Murray & Dickinson, 1996). Stability is enhanced not just *via* the mechanical strength of these films but also by electrostatic and steric repulsions by the interfacial materials, minimizing close approach of droplets limiting aggregation and coalescence.

Several studies indicate that interfacial films by proteins or their complexes exhibiting greater elasticity tend to effectively protect emulsion droplets against film rupture, and disproportionation, as well as restrict or delay lipolysis of droplets stabilized by the proteins/ their complex in the upper gastrointestinal phase (Miquelim, Lannes, & Mezzenga, 2010; Romoscanu & Mezzenga, 2005; Scheuble, Geue, Windhab, & Fischer, 2014). Notably, the physical properties of proteins are especially susceptible to environmental factors, such as pH, ionic strength, and temperature, which can compromise their stabilizing abilities (Chen, Yi, Zhang, Ding, Li, & Luo, 2022). Therefore, the formation of complexes between proteins and other food ingredients in order to modulate protein adsorption and stabilizing properties has been investigated in the literature (Araiza-Calahorra, Glover, Akhtar, & Sarkar, 2020; Araiza-Calahorra & Sarkar, 2019; Dai et al., 2018; Eichhorn, Thorenz, & Drusch, 2025; Hu & Xiong, 2022; Qin et al., 2022; Sarkar et al., 2018; Zhang, Murray, Suriyachay, Holmes, Ettelaie, & Sarkar, 2021a).

Recently, one combination of interfacial material that has become increasingly prevalent is plant-derived proteins + polyphenols, partly due to their ecologically friendliness and potential health-promoting properties (as well as their emulsifying capabilities) (Chen et al., 2022; Dai et al., 2020; Du et al., 2022; Han et al., 2022; Nimaming et al., 2024). As the trend advances towards greater use of plant-based materials, improving the functional properties of plant proteins by combining them with polyphenols seems particularly attractive.

Polyphenols can display interfacial activity on their own (Luo, Murray, Ross, Povey, Morgan, & Day, 2012; Luo, Murray, Yusoff, Morgan, Povey, & Day, 2011; Shishikura, Khokhar, & Murray, 2006; Zembyla, Murray, & Sarkar, 2018) and are recognized for their capacity to interact with proteins (either non–covalently or covalently) influencing the interfacial properties of the latter and therefore protein physicochemical behavior, including their emulsifying properties (Cheng et al., 2023; Nayak, Genot, Meynier, Dorlando, & Capron, 2022; Nimaming et al., 2024; Zembyla, Lazidis, Murray, & Sarkar, 2020; Zembyla, Murray, Radford, & Sarkar, 2019). Several investigations have shown that formation of hybrid particles between proteins and phenolic compounds *via* non-covalent interactions considerably enhances their capacity to stabilize oil droplets (Dai et al., 2020; Du et al., 2022; Ju et al., 2020; Li et al., 2020), although in most of these cases the complexes are presented as occurring between protein aggregate particles and polyphenol molecules, not polyphenol crystals. In our earlier work, spontaneous complex formation between potato protein (PoP) and quercetin crystals (QC) was demonstrated, building *so-called* hybrid PoPQC particles for the stabilization of Pickering emulsions (PE). The presence of QC-induced conformational changes in the PoP and PoPQC-stabilized PEs, resulting in outstanding long-term stability for several months (Nimaming et al., 2024).

Compared to pure protein adsorption, in such complexes, often part of the protein's hydrophobic regions that initiate adsorption are masked by the polyphenols, so that only

through structural rearrangement the proteins are expected to access the interface. In addition, interactions between the proteins and the polyphenols may enhance the viscoelastic interfacial film properties compared to those of the protein alone. At the same time, preservation of some of the 'particle-character' of the complexes may confer some of the natural advantages of Pickering stabilization, in terms of a high barrier to particle desorption and so high resistance to coalescence, Ostwald ripening and disproportionation unlike a molecularly adsorbed protein(Bock, Kieserling, Rohn, Steinhäuser, & Drusch, 2022; Cai et al., 2023; Hinderink, Sagis, Schroën, & Berton-Carabin, 2021; Ntone, van Wesel, Sagis, Meinders, Bitter, & Nikiforidis, 2021).

One key technique for examining structural re-arrangement and bond formation at interfaces is interfacial rheology, in particular interfacial shear rheology (Murray, 2002, 2011; Murray et al., 1996). The technique is frequently performed using a Couette rheometer fitted with bi-conical disk or double-wall ring geometries at the interface (Bertsch & Fischer, 2019; Chen et al., 2022; Eichhorn et al., 2025; Ikenaga & Sagis, 2024; Qin, Gao, & Luo, 2021; Su, Guo, Chen, Mao, Gao, & Yuan, 2020). A wide variety of interfacial and rheological investigations have been performed on various proteins over wide ranges of protein concentration, ionic strength, pH, temperature, and protein pretreatment, but relatively few on hybrid protein-flavonoid particles such as those discussed here. Overall, any factor that tends to decrease repulsion between the adsorbed entities tends to promote interfacial cross-linking and increase the film viscoelasticity. These factors may include changing the pH closer to the isoelectric pH (pI) of the proteins and/or increasing ionic strength (decreasing electrostatic repulsion). On the other hand, such changes may act in reverse by inhibiting the rearrangement of the different components adsorbed. Consequently, there is a need for further work on the understanding the behavior of protein–polyphenol complexes at interfaces, which this study seeks to address, specifically the case of PoPQC complexes. Also on consumption, the emulsions in the stomach encounter a significant

change in pH due to the extremely acidic gastric environment (pH 1–3) and are subjected to the action of the proteolytic enzyme pepsin by displaying the sites for peptic digestion as well as varying ionic conditions (Cao, Wang, & Xiong, 2025; Li, Ye, Lee, & Singh, 2012; Maldonado-Valderrama, Terriza, Torcello-Gómez, & Cabrerizo-Vílchez, 2013; Zhao et al., 2023). Hence, it was important to examine how understanding of interfacial properties of hybrid particles can be extrapolated to understand gastric digestion behavior of emulsions stabilized by PoPQC.

Therefore, the aim of this study was to understand the interfacial performance of plant protein-flavonoid hybrid particles under environmental conditions, as well as understand how those interfacial behavior translate into microstructural evolution of the emulsion droplets under *in vitro* gastric model. We used combination of tensiometry, interfacial shear rheology, emulsion sizing, microscopy and static digestion at varying pH and ionic conditions to compare the behavior of hybrid PoPQC particles versus non-hybrid PoP. Our hypothesis was PoPQC forms an elastic film at the interface and resilient to environmental conditions and therefore prevents the gastric coalescence of droplets stabilised by PoPQC.

2. Materials and methods

2.1 Materials

Potato protein isolate powder (PoP) from Sosa (“Potatowhip”) containing 90.5% protein which has been confirmed to be patatin-rich (Kew, Holmes, Stieger, & Sarkar, 2021), was purchased from Henley Bridge (Lewes, UK). Quercetin hydrate (Molecular weight (Mw) = 302.2 g/mol) in the form of crystalline, yellow-colored powder, was purchased from Fluorochem, Hadfield, UK. Sunflower oil (density and refractive index were 0.915 g/cm^3 at 25 ^{o}C and 1.470, respectively) was purchased from a local store (Tesco supermarket, UK). Florisil was used for oil purification (Fisher Scientific UK Ltd, UK). Pepsin from porcine gastric mucosa (P7000, activity of 371 U/mg) was purchased from Sigma-Aldrich Company

Ltd, Dorset, UK. The solvents used were of analytical grade. Milli-Q water (purified using Milli-Q apparatus refractive index = 1.333) with a resistivity of 18.2 MΩ cm at 25 °C (Millipore Corp., Bedford, UK) was used for preparation of the HEPES buffer (pH 7.0) and 0.1 M hydrochloric acid (HCl) or sodium hydroxide (NaOH) was used to adjust the pH. Sodium azide (SigmaAldrich, UK) at 0.02 wt% was employed as an antimicrobial agent.

2.2 Formation of potato protein (PoP) and hybrid potato protein-quercetin (PoPQC) particles

PoP and hybrid PoPQC solutions were prepared as described previously by Nimaming et al. (2024). Briefly, PoP powder (5.0 wt% total protein) was rehydrated with 20 mM HEPES buffer (pH 7.0) and stirred continuously for a minimum of 2 h to ensure complete dissolution of the protein. The crystalline QC powder was dissolved in pure ethanol (1.0 wt%) as a stock solution. In all hybrid samples, the mass ratio of PoP: QC in the PoPQC particles is depicted via abbreviations of the form PoPQCx: y, where x: y is the mass ratio between PoP and QC (w/w). Two ratios of hybrid PoPQC particles (PoPQC10: 1, and 10: 1.5) were prepared by slowly adding different volumes of the QC solution to 5.0 wt% of PoP solution at pH 7.0 under magnetic stirring, and ethanol was further evaporated. Sodium azide (0.02 wt%) was added as an antimicrobial agent.

2.3 pH and ionic strength treatments

PoP and both hybrid PoPQC particles were examined under various pH values and ionic strengths to investigate their interfacial behavior. The pH of samples (initially at pH 7.0) was adjusted between 3.0 to 9.0 by the addition of either 1.0 M HCl or 1.0 M NaOH (without any salt addition). For ionic strength variations, 20 mM HEPES + different NaCl concentrations

varying from 100 to 250 mM were prepared, and if necessary, the pH of solution was adjusted to 7.0.

2.4 Dynamic light scattering

Dynamic light scattering (DLS) was employed via a Malven Zetasizer Nano-ZS (Malvern Instruments, Malvern, UK) to measure the mean hydrodynamic diameter (d_H) of the PoP and hybrid PoPQC particles diluted to 1 mg/mL in standard disposable cuvettes. The absorption coefficient of the PoP and PoPQC was set as 0.001. The mean value of d_H, and the particle size distributions (PSD) are reported.

2.5 Oil purification

Sunflower oil was mixed with 5% (w/w) of Florisil® (60-100 mesh, Thermo Scientific Chemicals) and stirred overnight at room temperature to remove any surface-active impurities. The oil mixture was then centrifuged at 5,000×*g* for 15 min to remove the Florisil and the purified sunflower oil was collected and kept in the dark before further use.

2.6 Interfacial tension (*γ*) measurements

The interfacial tensions (γ) of PoP and hybrid PoPQC solutions/ dispersions at the purified sunflower oil-water (O/W) interface was measured *via* the pendant drop method at 25 °C using a DataPhysics OCA tensiometer (DataPhysics Instruments, Germany), following previous methodology (Akgonullu et al., 2024). Briefly, the needle was filled with samples (at a fixed total protein concentration of 0.5 wt%) before being immersed in a cuvette containing the purified sunflower oil. A 24 µL drop of the aqueous phase was formed at the tip of the needle and the drop profile was captured and evaluated via a CCD camera

connected to a computer running the SCA 20 program to extract and analyze the drop shape, which is then fitted to the Young-Laplace equation (equation (1)) to compute γ.

$$\Delta P = \gamma \left(\frac{1}{R_1} + \frac{1}{R_2} \right) \quad (1)$$

where ΔP ($P_{in} - P_{out}$) is the Laplace pressure across the interface, γ is the interfacial tension, and R_1 and R_2 are the principal radii of curvature, respectively.

The kinetics of adsorption was evaluated by measuring the initial slope of γ versus time (t), which corresponds to the diffusion-limited stage of adsorption. The plots of γ versus $t^{1/2}$ in this region exhibited linearity with the slope representing the diffusion rate constant (K_{diff}). A first-order rate equation can be calculated from equation (2) (Zhang et al., 2021b) to evaluate the rates of penetration/ adsorption and rearrangement of adsorbed material at the interface, represented as K_{ads} and K_{rear}, respectively:

$$\ln [(\pi_f - \pi_t) / (\pi_f - \pi_0)] = - k_i T \quad (2)$$

where, π_f, π_0, and π_t were the interfacial pressures at the final adsorption time, beginning time, and at any time throughout each stage, respectively, and k_i is the first-order rate constant. Surface pressure, $\pi = \gamma_0 - \gamma$, where γ_0 is the value of γ in the absence of any adsorbing material.

2.7 Interfacial shear rheology

Oscillatory interfacial shear rheology was performed with a modular compact rheometer (MCR-302, Anton Paar, Austria) fitted with biconical disk geometry (BiC68-5) at 25 °C

following the methodology of Akgonullu et al. (2024). The lower aqueous phase contained 0.1 wt% total protein, *i.e.*, considering whether the protein was on its own or as part of a PoPQC complexes. The bicone was lowered and positioned at the surface of the aqueous phase. Purified sunflower oil was then gently poured to form the upper oil layer to cover the lower aqueous phase. For time sweep measurements, the samples were observed over 16 h (57,600 s) at the constant angular frequency and strain of 6.283 rad/s, and 1%, respectively. Subsequently, amplitude sweeps were conducted at strains ranging from 0.01% to 100%, maintaining a constant angular frequency of 6.283 rad/s.

2.8 Pickering oil-in-water (O/W) and conventional emulsion preparation

Pickering emulsions stabilized by PoPQC10: 1 (E-PoPQC) and conventional emulsions stabilized by potato protein (E-PoP) as a control were prepared. The commercial sunflower oil was mixed with PoP or PoPQC dispersions at the ratio of 1: 4 (v/v), which in the final protein concentration of 1.0 wt% in emulsions. The mixtures were primarily produced by homogenization using an Ultra Turrax T25 homogenizer (IKA-Werke GmbH & Co., Staufen Germany) at 10,000 rpm for 1 min. The coarse emulsions were subsequently passed twice via the Leeds Jet Homogenizer (Two-chamber homogenizer, School of Food Science and Nutrition, University of Leeds, UK) at 300 bars pressure to produce fine emulsion droplets.

2.9 *In vitro* simulated gastric digestion

The static INFOGEST model for *in vitro* gastric digestion developed by Minekus et al. (2014) was applied. The procedure bypassed the oral phase owing to the absence of carbohydrates in the system. The behavior of the digested samples was determined by observing changes in droplet size (digested emulsion), and microstructure during digestion. The E-PoP or E-PoPQC (10 mL) at 37 ^{o}C was mixed with 10 mL of simulated gastric fluid (SGF) which

composed of 0.257 g/L of KCl, 0.061 g/L of KH_2PO_4, 1.05 g/L of $NaHCO_3$, 1.38 g/L of NaCl, 0.0122 g/L of $MgCl_2(H_2O)_6$, and 0.024 g/L of $(NH_4)_2CO_3$. The gastric digestion was simulated by adding the freshly prepared of pepsin (2000 U/mL), 5 µL of 0.3 M $CaCl_2$, and HCl for pH adjustment to pH 3.0. The simulated samples were incubated at 37 ^oC for 2 h using shaking incubator (400 rpm). The digested emulsions were systematically taken from the digested-SGF mixture at 5, 30, 60, 90, and 120 min to evaluate the droplet size, and microscopy analysis.

2.10 Droplet sizing

The droplet size of SGF-digested E-PoP and E-PoPQC as a function of gastric digestion time was measured using static light scattering using a Mastersizer (3000S series, Malvern Instruments Ltd, Malvern, UK). The average droplet size was reported as the volume mean diameter ($d_{4,3}$), and the full particle size distribution (PSD).

2.11 Confocal laser scanning microscopy (CLSM)

The Zeiss LSM 880 inverted confocal microscope (Carl Zeiss MicroImaging GmbH, Jena, Germany) was applied to evaluate the microstructure of *in vitro* gastric-digested E-PoP and E-PoPQC. The digested emulsions were stained using a Nile Red solution (1 mg/mL) for the oil phase, whereas Fast Green solution (1 mg/mL) was used to stain the protein phase. Nile Red and Fast Green were excited at wavelengths of 488 nm and 633 nm, respectively, while the excitation wavelength of autofluorescence of QC was at 405 nm. The stained emulsion samples were mixed with xanthan gum (1.0 wt%) to minimize the Brownian movement of oil droplets. Emulsion samples were dropped into a laboratory-fabricated well slide and thereafter gently covered with a coverslip (0.17 mm thickness) to avoid the entrapment of air bubbles. An oil immersion 63× objective lens was used to examine the emulsions.

2.12 Statistical analysis

Data are reported as means and standard deviations of either duplicate or triplicate samples prepared on independent days. The statistical analyses were conducted using one-way ANOVA and multiple comparison tests using SPSS software (IBM, SPSS statistics, version 24) and the significant difference between samples were considered when $p < 0.05$.

3. Results and discussion

3.1 Particle size

Influence of pH. We first examine the effect of pH (3, 5, 7 and 9) on the mean hydrodynamic particle diameter (d_H) of the PoP and hybrid PoPQC particles. Note that for all the particles, the particle size distribution (PSD) is quite broad (see **Fig. S1**). PoP exhibits the largest d_H of all, at pH 5 (**Fig. A1**), which can be attributed to this pH being close to isoelectric point of the main constituent, patatin, with isoelectric pH = 4.5 (Andlinger, Röscheisen, Hengst, & Kulozik, 2021; Bevan, Barker, Goldsbrough, Jarvis, Kavanagh, & Iturriaga, 1986; Guha, Majumder, & Mine, 2019). However, at all other pH values (3.0, 7.0 and 9.0) d_H for PoPQC10:1.5 >> d_H for PoPQC10:1 > d_H for PoP ($p < 0.05$). Thus, the interaction with QC seems to promote the creation of larger hybrid particles. Since our previous measurements have shown that the net zeta potential of these hybrid particles is greater than that of the PoP or QC alone (-26.17 mV for PoPQC10: 1, and -24.7 mV for PoPQC10: 1.5) (Nimaming et al., 2024), this suggests that QC somehow masks the net electrostatic repulsion between protein residues that keeps the PoP more separated when the pH is further away from the isoelectric point (pI) (~4.5-5.2), so that the proteins have a higher net charge. Additionally, it can be suggested that QC enhances hybrid particle formation via other forces, like hydrophobic interactions between QC at the surface of the particles, or QC-induced unfolded PoP (Nimaming et al., 2024), although some more specific interactions between particular functional groups on the protein or QC cannot be ruled out.

The PDI of PoP and hybrid PoPQC particles are broad, indicating considerable variation across all systems (see **Fig. A2**). For larger aggregates, particularly in the PoPQC10:1.5 where d_H exceeds 1 μm, DLS measurements may be influenced by sedimentation and multiple scattering effects. Therefore, the reported d_H is interpreted primarily as indicative of relative trends in aggregation behavior.

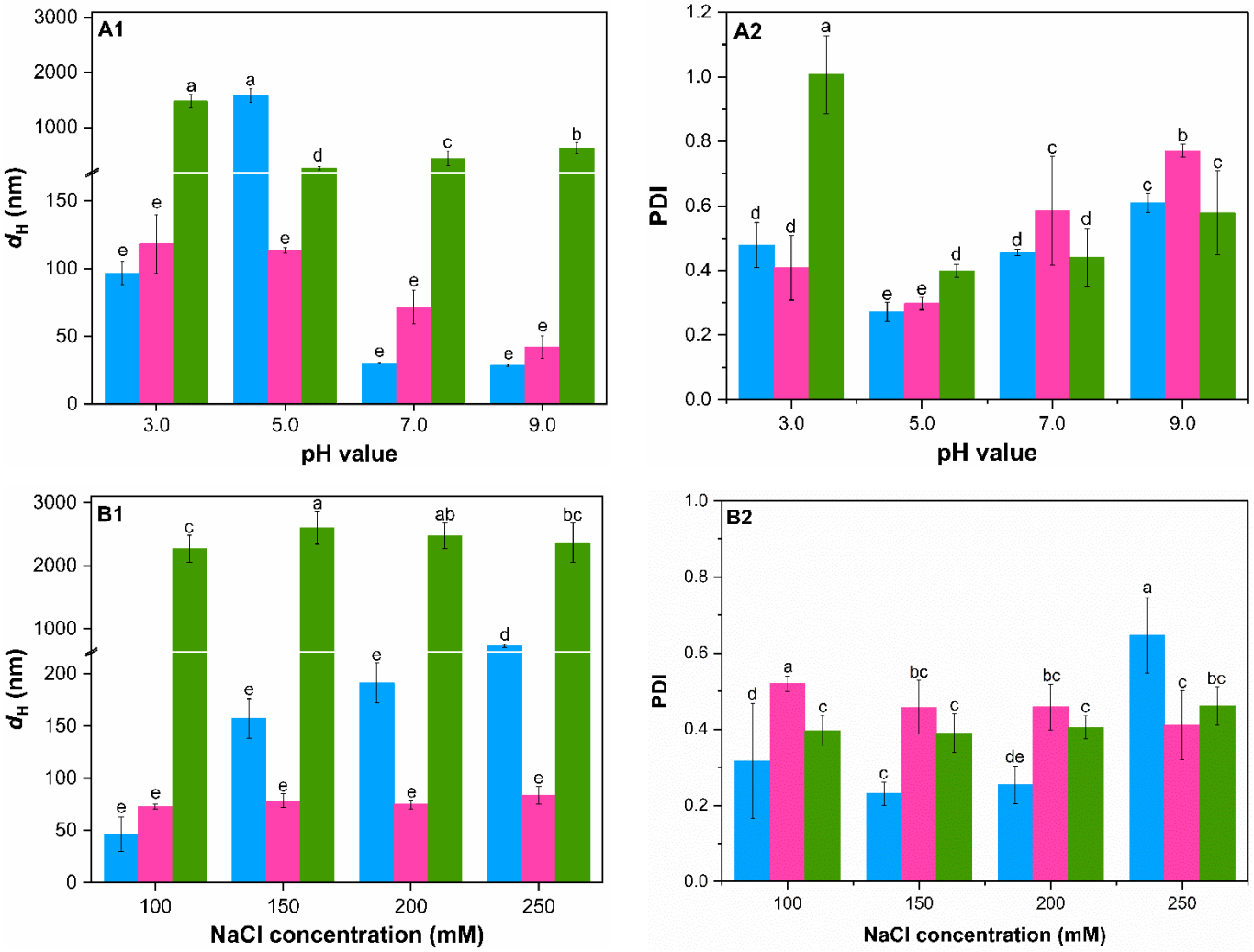

304

305 **Fig. 1.** Mean hydrodynamic diameter (d_H), and polydispersity index (PDI) of PoP (■), PoPQC10: 1 (■), and
306 PoPQC10: 1.5 (■) as function of pH (pH 3.0, 5.0, 7.0 and 9.0) (**A1-A2**), and ionic strength [NaCl] = 100, 150,
307 200 and 250 mM (**B1-B2**). Bars labelled with different lower-case letters are statistically different ($p < 0.05$)
308 based on Duncan's multiple range test. Data represents mean and error bars represent standard deviations
309 based on repeat measurements on three independent experiments (n = 3 × 3).

Influence of ionic strength. The effect of four different NaCl concentrations ([NaCl]= 100, 150 200 and 250 mM) on d_H of the particles at pH 7.0 was shown in **Fig. 1B**. **Fig. 1B** should be compared with **Fig. 1A**, particularly at pH 7.0 where no additional salts were included (**Fig. S2** gives the full PSDs and it is clear that these particle dispersions are very polydisperse). Nevertheless, for PoP, there is an increase in d_H with increasing [NaCl]. Since the PoP is charged, this is hardly surprising since increasing ionic strength screens electrostatic repulsion between protein molecules (Felix, Romero, Carrera-Sanchez, & Guerrero, 2019; Qin, Luo, Peng, Lu, & Zou, 2018; Zheng et al., 2023). What is noteworthy is that for the PoPQC10:1, d_H seems largely independent of [NaCl], considerably lower than for PoP alone and **Fig. S2B** shows that for these particles, there is only a single peak in the distribution, unlike for the PoP and PoPQC10:1.5 particles. The values of d_H for the other (PoPQC10:1.5) hybrid system are also relatively unaffected by [NaCl] but their d_H values are already very high (> 1 μm) and the PSDs are 'noisy', indicating that high aggregation states have been reached. Thus, the PoPQC10:1ratio appears to protect the PoP from excessive aggregation, yet remain insensitive to varying [NaCl] (Alghamdi, Birch, Vyshemirsky, & Rolinski, 2022; Yin et al., 2025; Zaplatic, Bule, Shah, Uddin, & Niaz, 2019). This again points the differences in the surface composition and/ or structure of the two types of hybrid particles and also the PoP aggregates themselves (*i.e*, alone), possibly due to hydrophobic interactions between QC at the surface of the particles, or QC-induced unfolding of PoP, as indicated earlier for the d_H results without added salt but as a function of pH.

The PDI of particles under varying ionic strengths showed broad size distributions (**Fig. B2**). The PoP showed significant aggregation at NaCl higher than 200 mM, while the hybrid PoPQC particles demonstrated greater stability, maintaining the most consistent profile across all ionic strengths.

3.2 Influence of pH on interfacial dynamics and shear rheology

Firstly, we wanted to clarify the dynamic reduction in tension followed by interfacial shear rheology as a function of pH and ionic strength both in POpQC as well as PoP. This will enable us to understand mechanistically the behavior of the interfacial film under gastric conditions.

Interfacial tension. **Fig. 2** (**A1, B1** and **C1**) shows the dynamic interfacial (γ) data plotted versus time ($t^{1/2}$) for PoP, PoPQC10:1 and 10:1.5, respectively, for analysis of the diffusive adsorption kinetic at shorter time scale (t = 100 s) (see **Fig. S3** for the raw γ versus time (t) data for PoP and the hybrid PoPQC particles at pH 3.0, 5.0, 7.0 and 9.0 up to ca. 2000 s adsorption time). **Fig. 2A2-C2** shows $ln\ [(\pi_f - \pi_t) / (\pi_f - \pi_0)]$ versus t for PoP, PoPQC10:1 and PoPQC10:1.5, respectively, for analysis of the longer time adsorption and re-arrangement kinetics (see eq. (1)). The general shape of the curves in **Fig. 2A1-C2** and **S3** are similar whilst **Fig. 2A3-C3** shows the fitted K_{diff}, K_{ads} and K_{rear} values as a function pH for the three types of particles – PoP (**Fig. 2A3**), PoPQC10:1 (**Fig. 2B3**) and PoPQC10:1.5 (**Fig. 2C3**). All values of K_{diff}, K_{ads}, K_{rear} and γ_{2000} are also given in **Table S1**. For all three particles, K_{diff} and K_{rear} are similar at all the tested pH values, in other words there seems to be no significant effect of the different d_H on the initial kinetics of adsorption as monitored by the fall in γ.

The only noticeable variation in kinetics seems to be reflected in the long-time re-arrangement constant K_{rear}. The K_{rear} seems overall lowest for PoPQC10:1, whilst for K_{diff} of PoP starts at similar values at pH 3.0 and 5.0 but then seems to increase somewhat at pH 7.0 and 9.0, indicating slightly slower rearrangement kinetics. For PoPQC10:1.5, K_{diff} is mostly higher than for PoPQC10:1 or PoP, except at pH 9.0 for PoP. It is difficult to interpret these differences other than to say that the main difference in the adsorption properties of the hybrid particles is that they seem to exhibit a difference in the longer-term re-arrangement of the species at the interfaces.

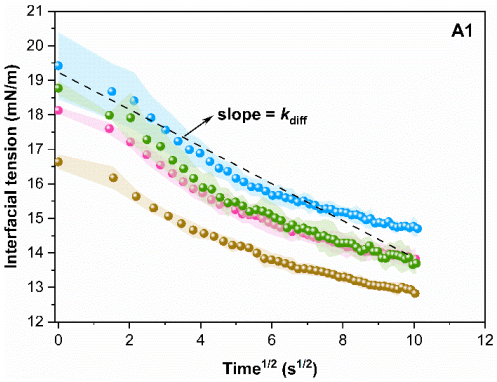
A1
slope = k_{diff}
Interfacial tension (mN/m)
Time$^{1/2}$ (s$^{1/2}$)

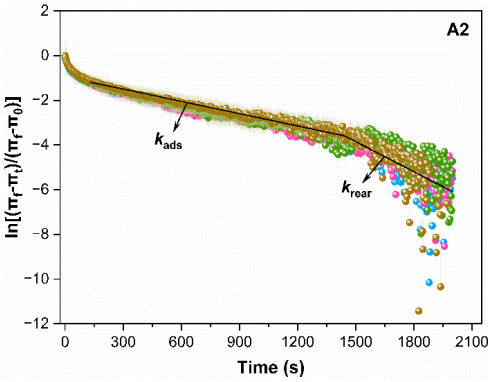
A2
k_{ads}
k_{rear}
ln[(π$_f$-π$_t$)/(π$_f$-π$_0$)]
Time (s)

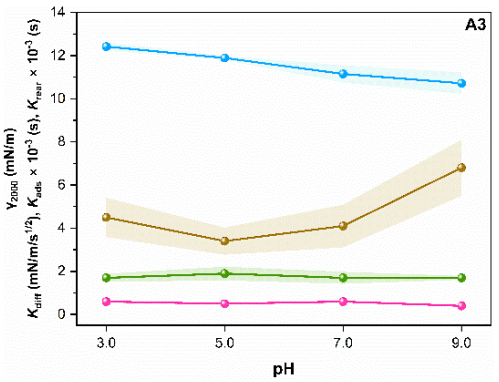
A3
γ_{2000} (mN/m)
K_{diff} (mN/m/s$^{1/2}$), K_{ads} × 10^{-3} (s), K_{rear} × 10^{-3} (s)
pH

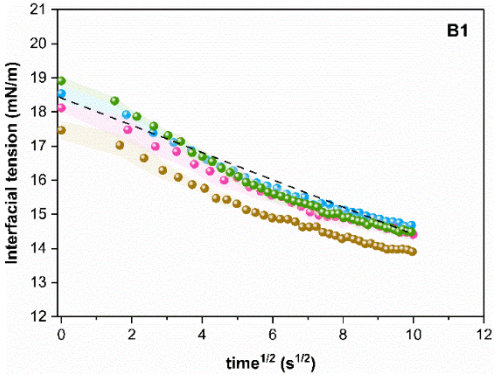
B1
Interfacial tension (mN/m)
time$^{1/2}$ (s$^{1/2}$)

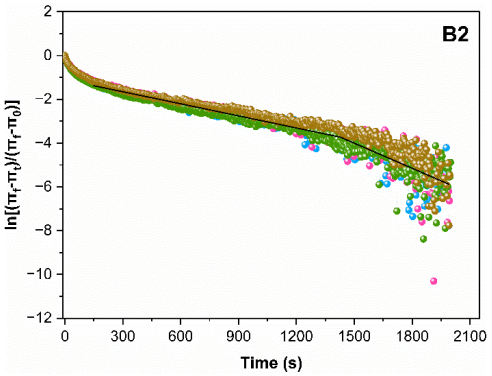
B2
ln[(π$_f$-π$_t$)/(π$_f$-π$_0$)]
Time (s)

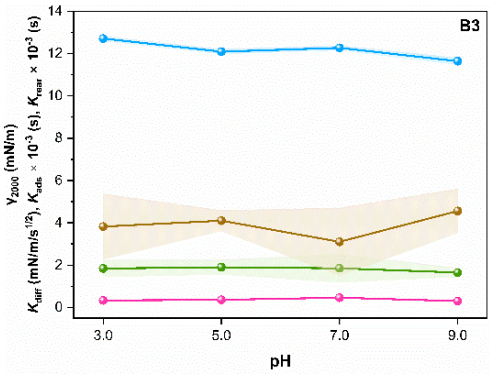
B3
γ_{2000} (mN/m)
K_{diff} (mN/m/s$^{1/2}$), K_{ads} × 10^{-3} (s), K_{rear} × 10^{-3} (s)
pH

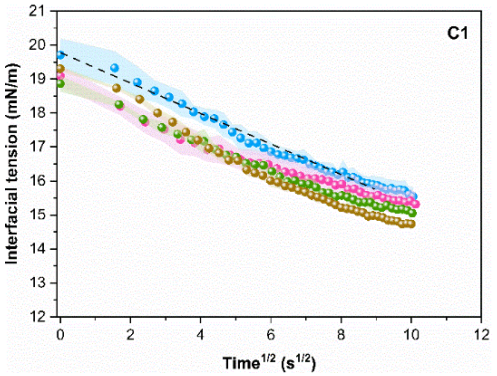
C1
Interfacial tension (mN/m)
Time$^{1/2}$ (s$^{1/2}$)

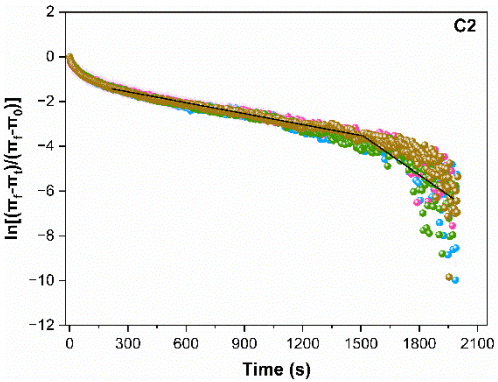
C2
ln[(π$_f$-π$_t$)/(π$_f$-π$_0$)]
Time (s)

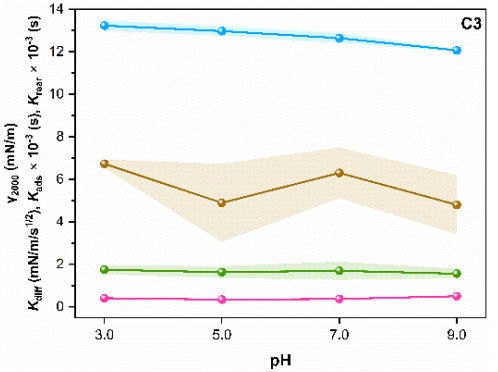
C3
γ_{2000} (mN/m)
K_{diff} (mN/m/s$^{1/2}$), K_{ads} × 10^{-3} (s), K_{rear} × 10^{-3} (s)
pH

361

Fig. 2. Interfacial tension (γ) versus $t^{1/2}$ (where t = adsorption time) (**1**) of PoP (**A**), PoPQC10:1 (**B**), and PoPQC10:1.5 (**C**) at different pH values: pH 3.0: ●, pH 5.0: ●, pH 7.0: ● and pH 9.0: ●. The dashed line shows a linear fit of γ versus $t^{1/2}$, with a slope = K_{diff} and corresponding γ versus t over 2000s (**2**) with fitted values of K_{ads} and K_{rear}, respectively. Mean γ at t = 2000 s (γ_{2000}) (●), K_{diff} (●), K_{ads} (●), and K_{rear} (●) (**3**) as a function of pH for PoP (**A**), PoPQC10:1 (**B**) and PoPQC10:1.5 (**3**), extracted from Figs. 2A1-C2. The shading represents standard deviations based on repeat measurements on three independent experiments (n = 3 × 3).

This is somewhat in agreement with the γ_{2000} values, which are almost the same at all pH values but slightly lower for PoP, particularly at the high pH values (7.0 and 9.0) where K_{rear} is highest, *i.e.*, the particles continue to rearrange for longer time to lower γ further, which is expected primarily due to their larger size (**Fig. 1A**). Nevertheless, other effects such as charge distribution, hydrophobicity, which are further impacted by pH changes cannot be ignored in the interfacial dynamics.

Interfacial shear rheology. **Fig. 3** shows the dynamic interfacial storage modulus G_i' versus t (**Figs. 3A1, B1** and **C1**) for the three particle types at pH 3.0, 5.0, 7.0 and 9.0, for comparison with γ results discussed above. Corresponding G_i' versus interfacial shear strain (s_i) plot are shown in **Figs. 3A2, B2** and **C2** for the films at t = 30 min. As with the γ results, the general shape of all the G_i' versus t curves is the same, G_i' showing a rapid increase followed by a smooth slowing down and almost levelling off to a constant value after ca. 900 s. Similarly, all the G_i' versus s_i curves have the same sort of trend, with G_i' constant up to ca. s_i = 1 %, followed by a sharp drop in G_i', indicating significant weakening or fracture of the interfacial films. By analogy with **Fig. 2A3-C3**, it is easier to highlight differences between the systems in terms of a summary plot – this case **Fig. 3A3-C3**. The **Figs. 3A3-C3** show the values of G_i' after 960 min and the values of the critical strain, γ_{crit}, at pH 3.0 and 5.0, where noticeable yielding of the films was considered to occur. These γ_{crit} values were obtained by averaging the G_i' data between γ = 0.01 and 1 in each case and

taking γ_{crit} as the first value of γ at which G_i' had dropped to 90% of this value (Lavoisier, Vilgis, & Aguilera, 2019). Again, these values for the three different particles and the four different pH values are also tabulated in **Table S2**.

Figs. 3A3-C3 show that the G_i' values after 960 mins at pH 3.0 and 5.0 are different. The G_i' value for PoP, PoPQC10:1 and PoPQC10:1.5 always peaked at pH 5, *i.e.*, closest to the pI of PoP, as mentioned earlier (G_i' increases from pH 3.0 to 5.0). It is well known that interfacial shear viscoelasticity for proteins tends to be highest at around the pI, when intermolecular repulsion is lowest and therefore intermolecular cross-linking is more likely (Dickinson, 1998; Kieserling, Pankow, Keppler, Wagemans, & Drusch, 2021; Murray, 2002; Rühs, Scheuble, Windhab, Mezzenga, & Fischer, 2012). However, the highest G_i' values at pH 5.0 (and pH 3.0) are seen for the PoPQC10:1 (**Fig. 3B3**), not for pure PoP (**Fig. 3A3**). This suggests that the formation of the complex with QC induces conformational changes in the PoP as evidenced by previously through small angle X-ray scattering, circular dichroism (Nimaming et al., 2024), which can lead to reduced interactions close to pI. It is also noticeable that the PoP system shows the largest variation (decrease) in γ_{crit}, whilst the corresponding values of G_i' slightly increase from pH 3.0 to pH 5.0. Weaker interfacial films are often seen to be more deformable before they break, by analogy with bulk material that is very rigid but brittle. For PoPQC10:1, γ_{crit} stays constant between pH 3.0 and 5.0, however, γ_{crit} of PoPQC10:1.5 decrease from pH 3.0 same as PoP system. At present we cannot find a obvious link between this trend and the other measured characteristics of the adsorbed films, though it should be noted that the definition of γ_{crit} is necessarily arbitrary. These results are in line with the findings of interfacial properties of patatin-rich potato protein (neutral pH), and protease inhibitor-rich potato protein (pH 3.6), and other plant proteins investigated by Ikenaga et al. (2024). The increased and reduced G_i' of PoP obtained from low and high pH values (5.0 and 9.0) also corresponded with the observation

of hazelnut protein (Gul, Gul, Baskıncı, Parlak, & Saricaoglu, 2023), and faba bean protein (Felix et al., 2019).

To conclude this section, it is obvious that pH is crucial in determining the interfacial strength of the films formed from the different particles. This s_i is in contrast to the γ results, which were relatively insensitive to the particle type and conditions. However, this is not surprising since it is well known that interfacial shear rheology is much more sensitive to the interactions between the adsorbed film components, whereas γ is more a measure of interfacial coverage.

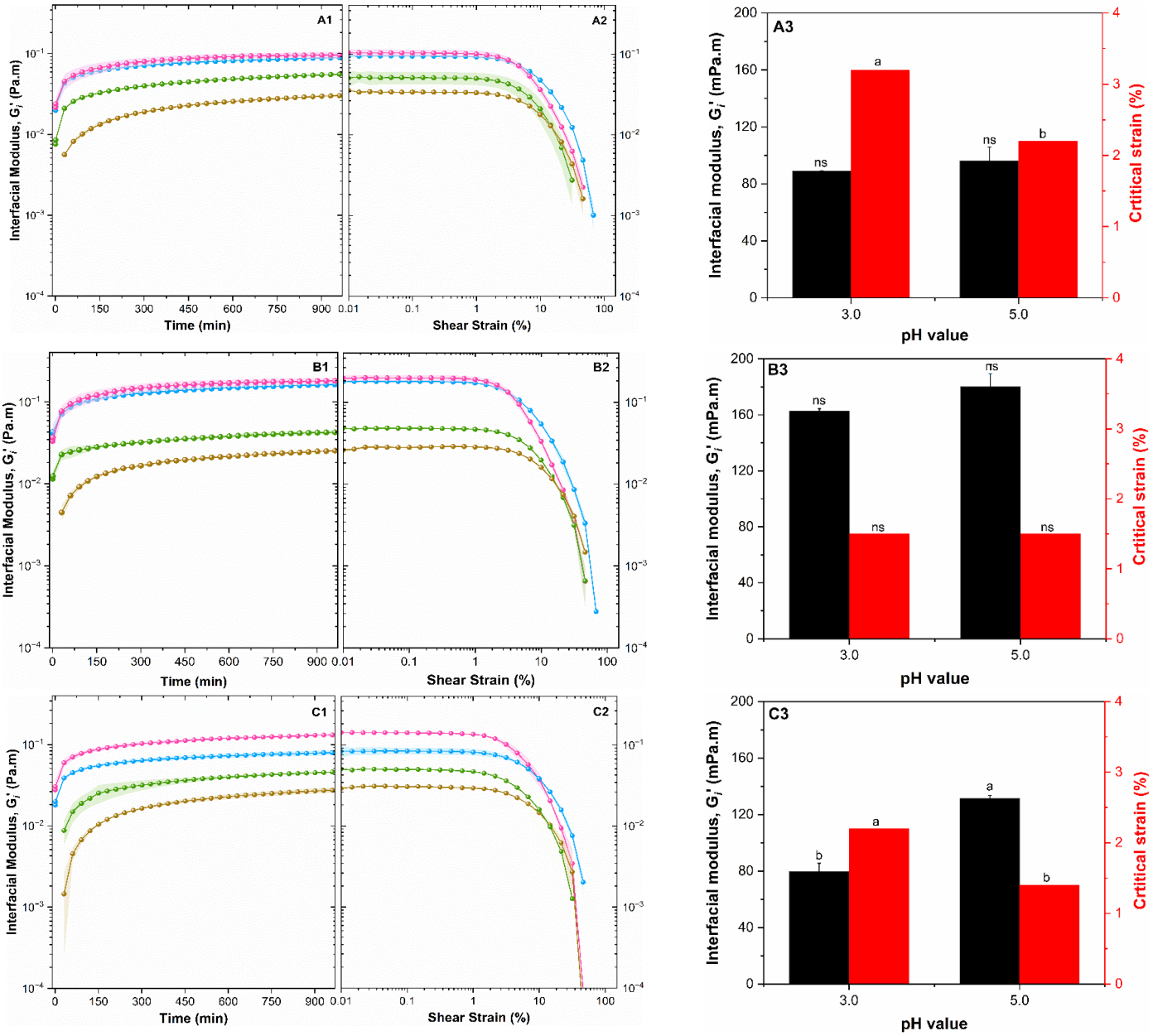

Fig. 3. Interfacial storage modulus (G_i') versus adsorption time (t) (**1**) and shear strain (**2**) of PoP (**A**), hybrid PoPQC10:1 (**B**), and PoPQC10:1.5 particles (**C**) at pH 3.0 (●), pH 5.0 (●), pH 7.0 (●) and pH 9.0 (●). Interfacial storage modulus (G_i'; ■) at 960 min, and critical strain (%) (■), measured at 1 Hz (**3**) of PoP (**A**), hybrid PoPQC10: 1 (**B**), and PoPQC10:1.5 (**C**) particles at pH 3.0 and 5.0 extracted from **A1-C2**. Bars labelled (**3**) with different lower-case letters $^{(a\text{-}b)}$ are statistically different ($p < 0.05$), and ^{ns} indicates mean values are non-significant differences ($p \geq 0.05$) based on Duncan's multiple range test. Error bars represent standard deviations based on repeat measurements on three independent experiments (n = 2 × 2).

3.3 Influence of ionic strengths on interfacial dynamics and shear rheology

Interfacial tension. **Figs. 4A1-C1** shows the γ data plotted versus $t^{1/2}$ for PoP, PoPQC10: 1 and PoPQC10:1.5, respectively, for analysis of the diffusive adsorption kinetic at short time (t = 100 s) (**Fig. S4** shows the raw γ versus time (t) data for PoP and the hybrid particles at pH 7.0 with the four different added [NaCl] as in **Fig. S3** for the four different pH values without additional NaCl). **Figs. 4A2-C2** show ln [$(\pi_f - \pi_t) / (\pi_f - \pi_0)$] versus t for PoP, PoPQC10:1 and PoPQC10:1.5, respectively, for analysis of the longer time adsorption and re-arrangement kinetics (see eq. (1)). **Figs. 4A1-C2** can therefore be compared with **Figs. 2A1-C2**, whilst **Figs. 4A3-C3** show the K_{diff}, K_{ads} and K_{rear} values fitted to the curves in **Figs. 4A1-C2**, for comparison with the same parameters plotted in **Figs. 2A3-C3** as a function of pH. Once again, we have tabulated all these values in the Supplementary Information (see **Table S3**). Also shown are the 'final' values of γ after t = 2000 s.

Comparing **Figs. 4A3-C3** with **Figs. 3A3-C3**, none of the fitted rate constants or γ_{2000} values differ much across systems, *i.e.*, in particular K_{diff}, K_{ads} and γ_{2000} seem rather insensitive to pH and [NaCl] for all the three systems i.e. hybrid particles versus non-hybrid PoP. There is a slight decrease in γ_{2000} with increasing [NaCl] for all three samples which might indicate reduced electrostatic screening, aiding adsorption by reducing mutual repulsion between species that have already adsorbed and between these and species trying to adsorb, which is a well-known effect. The K_{rear} shows the largest variation with [NaCl] for any particle type but again it is hard to draw any form of connections between the slight increases and decreases as a function of [NaCl] for the different particle and any other measured characteristics of the adsorbed films, other than that it is the longer term rearrangement that are more sensitive to the different ionic strength.

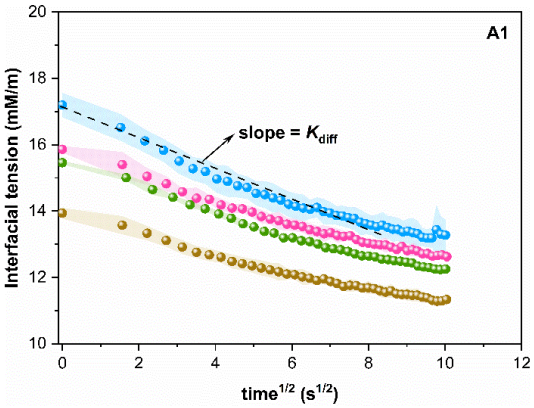
A1
slope = K_{diff}
Interfacial tension (mM/m)
time$^{1/2}$ (s$^{1/2}$)

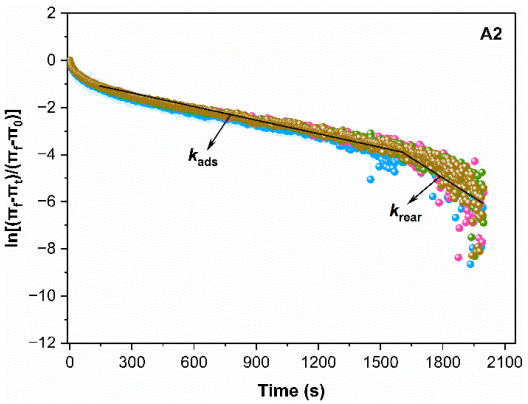
A2
k_{ads}
k_{rear}
ln[(π$_f$-π$_t$)/(π$_f$-π$_0$)]
Time (s)

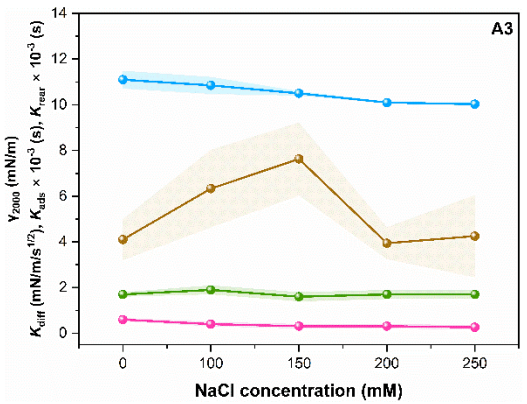
A3
K_{diff} (mN/m/s$^{1/2}$), K_{ads} × 10^{-3} (s), K_{rear} × 10^{-3} (s)
γ$_{2000}$ (mN/m)
NaCl concentration (mM)

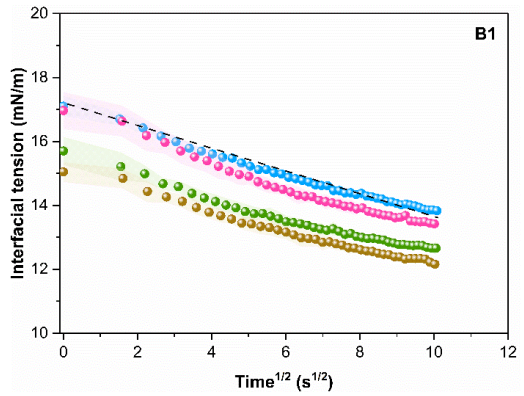
B1
Interfacial tension (mN/m)
Time$^{1/2}$ (s$^{1/2}$)

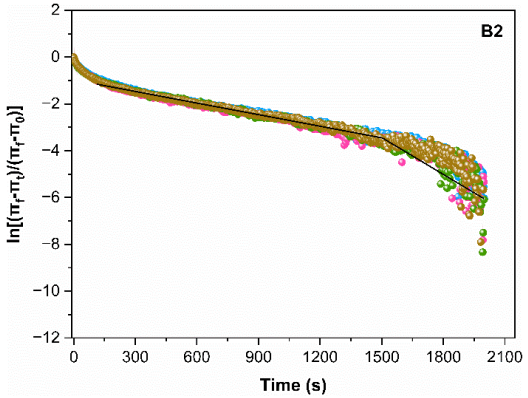
B2
ln[(π$_f$-π$_t$)/(π$_f$-π$_0$)]
Time (s)

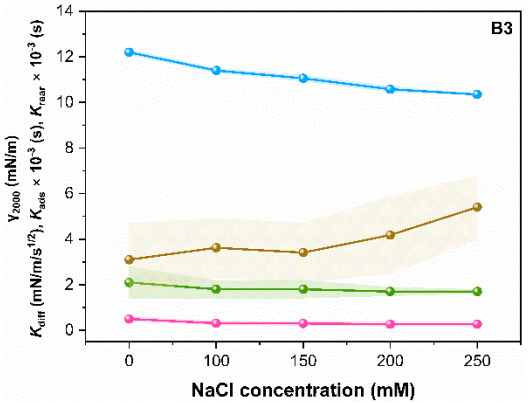
B3
K_{diff} (mN/m/s$^{1/2}$), K_{ads} × 10^{-3} (s), K_{rear} × 10^{-3} (s)
γ$_{2000}$ (mN/m)
NaCl concentration (mM)

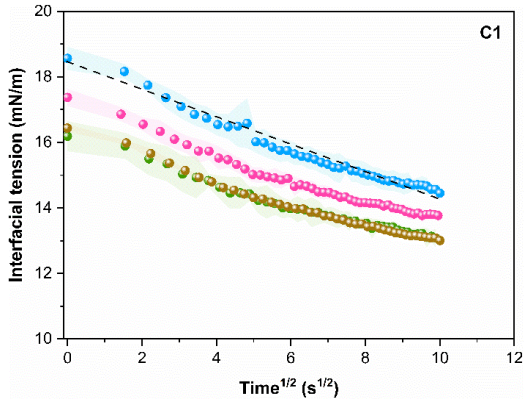
C1
Interfacial tension (mN/m)
Time$^{1/2}$ (s$^{1/2}$)

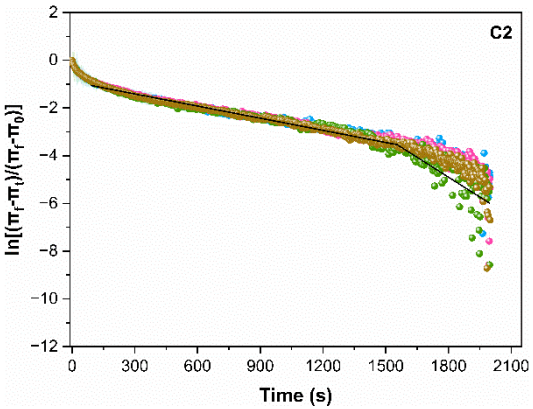
C2
ln[(π$_f$-π$_t$)/(π$_f$-π$_0$)]
Time (s)

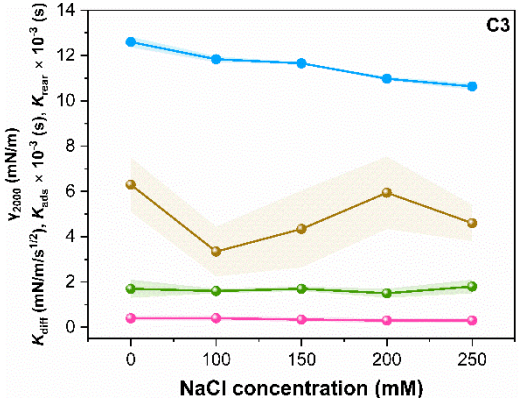
C3
K_{diff} (mN/m/s$^{1/2}$), K_{ads} × 10^{-3} (s), K_{rear} × 10^{-3} (s)
γ$_{2000}$ (mN/m)
NaCl concentration (mM)

Fig. 4. Interfacial tension (γ) versus $t^{1/2}$ (where t = adsorption time) (**1**) of PoP (**A**), PoPQC10:1 (**B**), and PoPQC10:1.5 (**C**) at different [NaCl]: 100 mM (●), 150 mM (●), 200 mM (●) and 250 mM (●). Also shown is the fit to γ versus $t^{1/2}$, the slope = K_{diff} and corresponding γ versus t over 2000s (**2**) with fitted values of K_{ads} and K_{rear}, respectively. Mean γ at t = 2000 s (γ_{2000}) (**1**) (●), K_{diff} (●), K_{ads} (●), and K_{rear} (●) as a function of [NaCl] for PoP (**A**), PoPQC10:1 (**B**) and PoPQC10:1.5 (**C**), extracted from **Fig. 4A1-C2**. The shading in slightly light color represents standard deviations based on repeat measurements on three independent experiments (n = 3 × 3).

Interfacial shear rheology. **Fig. 5** shows the dynamic interfacial storage modulus G_i' versus t (**Figs. 5A1-C1**) for the three particle types at [NaCl] = 100–250 mM, for comparison with γ results discussed above. Also shown (in **Figs. 5A2-C2**) are the corresponding G_i' versus interfacial shear strain (s_i) plot for the films at t = 30 min. Thus **Figs. 5A1-C2** can be compared with **Fig. 3A1-C2** earlier, which shows the same parameters with no added NaCl. Overall, the shapes of G_i' vs t and G_i' vs s_i plots look very similar, except that the curves for the different [NaCl] are somewhat closer together. Again, it is easier to analyze any trends with a summary plot, so **Figs. 5A3-C3** plot the values of G_i' after 960 min and the values of the critical strain γ_{crit} at which significant yielding or fracture of the films is considered to occur, obtained from the raw data in **Figs. 5A2–C2**, for comparison with **Figs. 3A3-C3**.

It can be seen in **Figs. 5A3-C3** that G_i' after 960 min for PoP was effectively between [NaCl] = 100 to 200 mM, within experimental error, although all these values were slightly lower than without adding NaCl at pH 7.0 (see **Fig. 5A3**). On the other hand, the value of γ_{crit} at 100 is somewhat lower than the value without salt (*i.e.* the interfacial films were more brittle) but at 200 mM, this γ_{crit} value increases back to almost the same value as zero added NaCl. This variation in γ_{crit} is in marked variation to the behavior with the PoPQC10:1 and PoPQC10:1.5 hybrid particles, which show virtually no change in γ_{crit} with increasing [NaCl]. In addition, the hybrid PoPQC10:1 and PoPQC10:1.5 particles show an *increase* in G_i' as [NaCl] increases from 100 mM higher [NaCl], peaking at 200 mM for both PoPQC10:1 and

PoPQC10:1.5 particles. Remarkably, the G_i' values for the hybrid particles are higher at [NaCl] > 100 mM, which is higher than with no added salt. Thus, overall, the higher ionic strengths at pH 7.0 appears to strengthen the adsorbed films of the hybrid particles, but not the PoP aggregates. In general, increasing ionic strength tends to strengthen interfacial films up to a point (Feng, Wang, Wang, Xia, & Huang, 2021), unless the ionic strength becomes so high that protein solubility start to become compromised (Murray, 2011). Whether the increase observed here is due to enhanced screening of the electrostatic repulsion between the adsorbed species or enhanced re-arrangement within the adsorbed films, promoting interfacial cross-linking, is not clear at present, but it again indicates more complex interactions between the adsorbed hybrid particles that are more easily detected in the interfacial rheology measurements than the interfacial tension measurements. Certainly, this corresponds to the larger d_H of the PoPQC10:1.5 particles (**Fig. 1**), indicating greater aggregation in the bulk, but not the PoPQC10: 1 particle, which apparently remains more or less the same size, at least in the bulk phase.

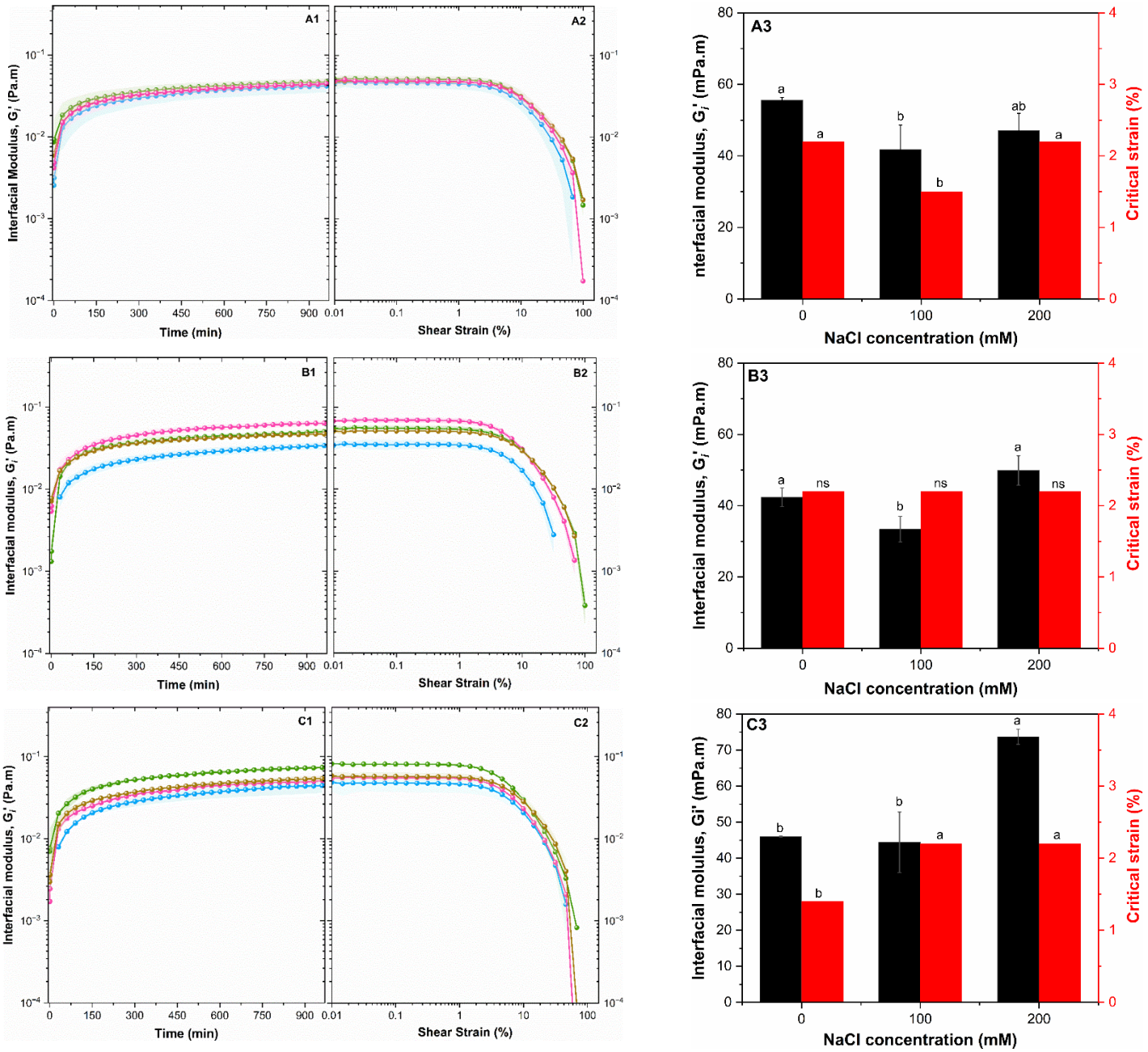

496

497 **Fig. 5.** Interfacial storage modulus (G_i') versus adsorption time (*t*) (**1**) of PoP (**A**), hybrid PoPQC10:1 (**B**), and
498 PoPQC10:1.5 (**C**) hybrid particles at different [NaCl]: 100 mM (●), 150 mM (●), 200 mM (●) and 250 mM (●) at
499 pH 7.0 and corresponding plots of G_i' versus shear strain (s_i) measured at 1 Hz (**2**). **I**nterfacial storage modulus
500 (G_i'; ■) at 960 min, and critical strain (%) (■), measured at 1 Hz at pH 7.0 (**3**) for PoP (**A**), hybrid PoPQC10:1
501 (**B**) and PoPQC10:1.5 (**C**) particles at 0, 100, and 200 mM NaCl extracted from **Figs. 5A1-C2**. Bars labelled
502 (**3**) with different lower-case letters $^{(a\text{-}b)}$ are statistically different ($p < 0.05$), and ^{ns} indicates mean values are
503 non-significant differences ($p \geq 0.05$) based on Duncan's multiple range test. The shading in slightly light color
504 represents standard deviations based on repeat measurements on three independent experiments (n = 2 × 2).

3.4 *In vitro* gastric digestion of emulsions

Having understood the interfacial behaviour of the hybrid particular verusus PoP film, we now examined the behavior of Pickering emulsions stabilized by hybrid PoPQC particles, particularly under harsh environments such as *in vitro* gastric conditions. Prior to gastric digestion, the volume-average mean diameter ($d_{4,3}$) of the emulsion stabilized by PoP (E-PoP) and the emulsion stabilized by PoPQC (E-PoPQC) was about 2 μm and 9 μm **(Table 1.**), respectively, which was comparable in sizes to previous study (Nimaming et al., 2024). The initial droplet size distribution of E-PoP at pH 7.0 was monomodal with a main peak lying between 3 to 50 μm (**Fig. 6A**), while E-PoPQC exhibited polymodal distributions, with the primary peak in the range of 3 to 100 μm and the smaller peaks below 3 μm (**Fig. 6B**). The presence of those small peaks was evident in CLSM micrographs as seen in **Fig. 7B**, indicating some small droplet and unabsorbed PoPQC. The CLSM images also showed flocculated oil droplets, those stabilized by PoPQC. The incubation in SGF without pepsin had a slight impact causing increase in $d_{4,3}$ of E-PoP, and decrease in $d_{4,3}$ of E-PoPQC ($p < 0.05$).

In the presence of SGF containing pepsin, the main peak of size distributions of E-PoP shifted to larger droplet size indicating droplet coalescence, and the $d_{4,3}$ values of E-PoP increased considerably ($p < 0.05$) (**Table 1.**). The small peaks appeared below 1 μm (**Fig. 6A**), which might be attributed to the smaller size of digested and/ or proteolysis of the unabsorbed proteins. Several factors could be attributed to droplet coalescence or flocculation, but primarily (i) the interfacial protein-coated oil droplets were entirely or partly hydrolyzed by pepsin that were not of sufficient film thickness and viscoelasticity to offer resistance against coalescence (Yang, Zhi, W., Paul, Harjinder, & and Ye, 2025; Zhou, Lin, Xu, Meng, & Dong, 2020); whilst other minor factors could be (ii) the charge of proteins at droplet surfaces were modified at low pH; and (iii) the ion screening effects caused by ionic strengths in the gastric conditions (Sarkar, Goh, Singh, & Singh, 2009; Sarkar, Zhang,

Holmes, & Ettelaie, 2019; Singh & Sarkar, 2011; Singh, Ye, & Ferrua, 2015; Singh, Ye, & Horne, 2009). The evidence of flocculation and coalescence of droplets were also detectable in the CLSM images (**Fig. 7A**) at 60 min and prolonged digestion time as observed in previous studies (Li et al., 2020; Liu et al., 2021; Zou et al., 2017). It had been reported previously that extending digestion time with the presence of pepsin promotes the rapid hydrolysis of absorbed PoP at the droplet interface into small molecule polypeptides, resulting in relatively intact PoP remaining on the emulsion interfaces after 10 minutes of digestion (Li et al., 2012). Interestingly, the E-PoP size distributions between 60 and 120 min exhibited no significant difference ($p > 0.05$), implying that proteins were mostly digested by pepsin within the first hour of gastric digestion time. The PoP network becomes almost invisible around the 120-min period of *in vitro* gastric digestion, as seen by a reduction in the green signal (**Fig. 7A**), indicating that the residual proteins had been fully digested and diluted since the gastric environment is now far away from the isoelectric point of the proteins.

Conversely, the E-PoPQC showed slightly smaller droplets under gastric digestion ($p < 0.05$). The $d_{4,3}$ significantly decreased from 7.50 μm to 6.67 μm (**Table 1**), and the main peak of size distributions were slightly moved to the left (smaller droplets) within 2-h gastric digestion. Some droplets were partially broken down into smaller sizes during gastric digestion; nevertheless, the main peaks remained within the same range before digestion. This is attributed to the hybrid PoPQC particle-rich interfacial layer efficiently restricting the access of pepsin to the adsorbed layers. The microstructure of the digested E-PoPQC showed that mostly droplets remained unaffected at the end of gastric digestion (120 min) (**Fig. 7B**). The complex interfacial structure of the hybrid PoPQC particles (**Figs. 2-5**) potentially hindered the droplet coalescence in gastric condition unlike the PoP. Noteworthy, QC is known to bind to pepsin *via* hydrophobic interactions and reduce its activity (Hashemi-Shahraki, Shareghi, & Farhadian, 2023). The contribution of free QC in the continuous

phase in this particular concentration reducing the activity of pepsin in the *in vitro* gastric model is beyond the scope of this work and needs further investigation in the future. Therefore, the complex interface created by PoPQC, network formation between PoP and QC bridging on the droplet surfaces as well as potential contribution diminishing the activity of pepsin from QC in the continuous phase might have played a key role in preventing the droplet coalescence under the *in vitro* simulated gastric digestion.

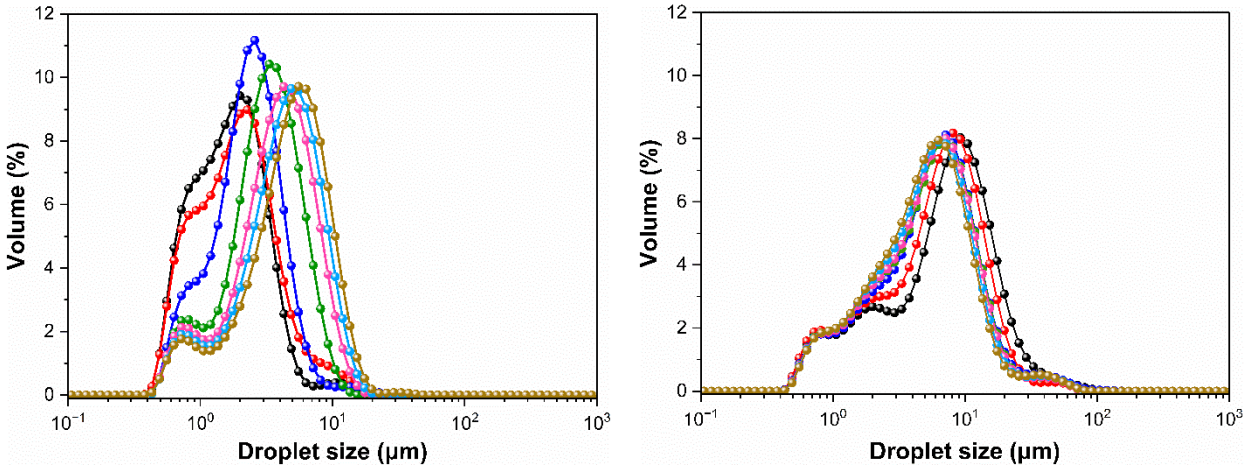

Fig. 6. Mean droplet size distributions of E-PoP (**A**), and E-PoPQC (**B**) under *in vitro* gastric digestion at different digestion times. Initial emulsion (pH 7.0) before adding SGF (●), gastric phase at 0 min (emulsions were mixed with SGF without the addition of pepsin, ●), 5 min (●), 30 min (●), 60 min (●), 90 min (●), and 120 min (●). Data are represented as average based on three independent readings on triplicate samples (n = 3 × 3).

Table 1. Evolution of mean droplet size (± standard deviation) of E-PoP and E-PoPQC under *in vitro* gastric digestion at different time points.

Digestion time	**E-PoP** ($d_{4,3}$, μm)	**E-PoPQC** ($d_{4,3}$, μm)
initial emulsion (pH 7.0)	2.03 ± 0.04^{gB}	9.18 ± 0.19^{aA}
+ SGF (no pepsin)	2.41 ± 0.09^{fB}	7.72 ± 0.19^{bA}
5 min	2.67 ± 0.07^{eB}	7.50 ± 0.26^{cA}
30 min	3.53 ± 0.20^{dB}	7.06 ± 0.14^{dA}

60 min	4.35 ± 0.32^{cB}	6.96 ± 0.15^{deA}
90 min	4.91 ± 0.38^{bB}	6.81 ± 0.19^{efA}
120 min	5.50 ± 0.34^{aB}	6.67 ± 0.16^{fA}

571 Mean values with different lowercase letters $^{(a-g)}$ with the same column, and uppercase letters $^{(A-C)}$ with the
572 same row indicate significant differences ($p < 0.05$) based on Duncan's multiple range test.

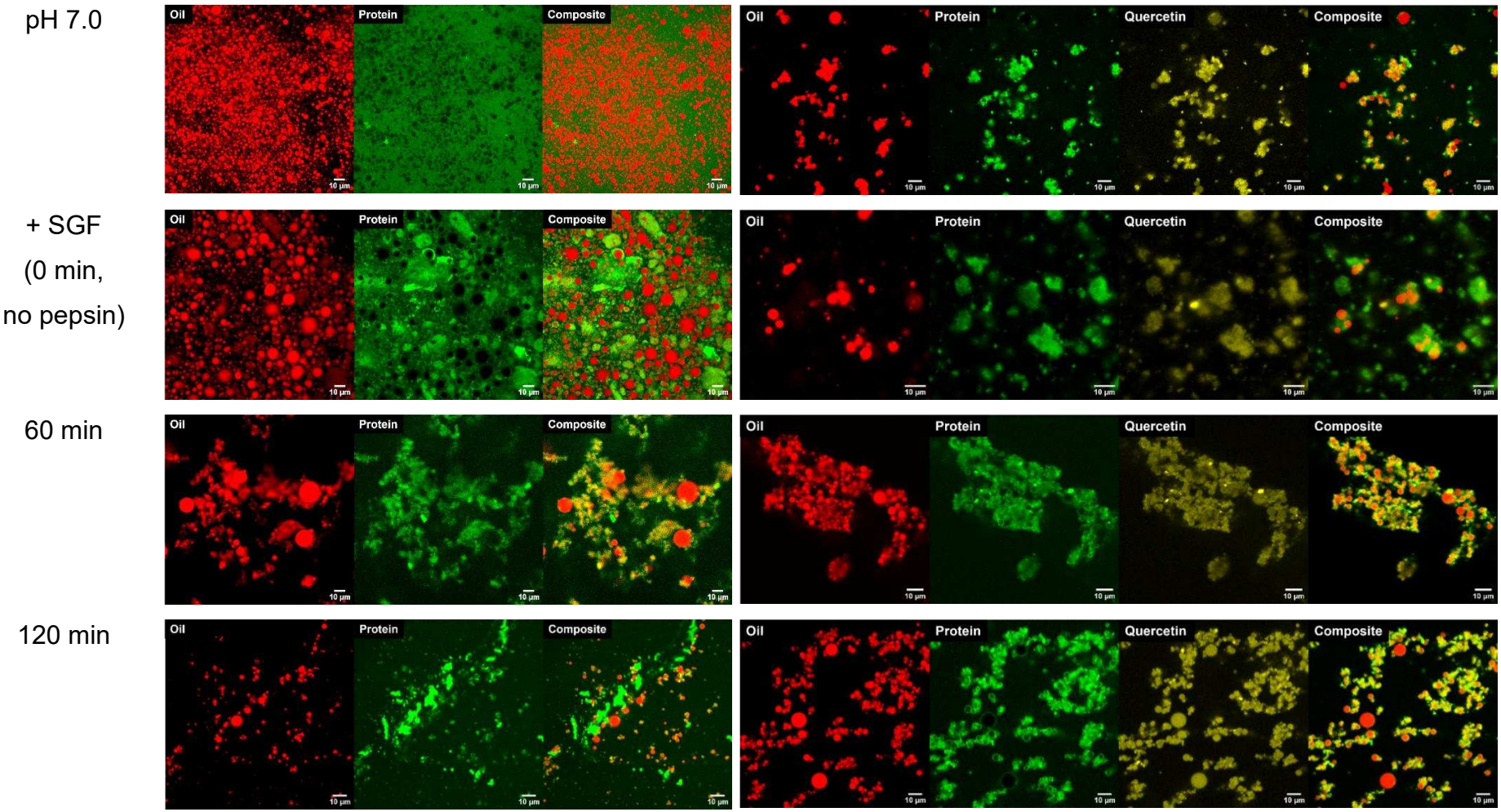
Digestion time
(A) E-PoP
(B) E-PoPQC
pH 7.0
+ SGF (0 min, no pepsin)
60 min
120 min
Oil
Protein
Quercetin
Composite
10 μm

573

Fig. 7. Confocal images of *in vitro* gastric digestion of E-PoP (**A**), and E-PoPQC (**B**) at different digestion times. Red (Nile Red stain) and green (Fast Green stain) colors represent the oil and protein phase; whilst quercetin is auto fluoresced with excitation of 405 nm. The composite was a merge channel of all channels. The ‘‘pH 7.0’’ denoted the initial emulsion droplet prior digestion without the addition of SGF and pepsin. The digestion time of ‘‘+ SGF (0 min, no pepsin)’’ indicated the emulsion was mixed with SGF mixture (pH 3.0) without the presence of pepsin. The digestion time of 60, and 120 min corresponded to digestion periods under *in vitro* gastric digestion, respectively. The scale bar was 10 μm.

4. Conclusions

This work elucidated the interfacial properties of hybrid PoPQC particles compared with native PoP as a function of pH and ionic strength, alongside the *in vitro* simulated gastric digestion of the emulsions stabilized by these materials. The hybrid dispersions showed minor variations in particle size between pH 3.0–9.0, with limited aggregation at pH 5.0 unlike PoP. Meanwhile, the hybrid PoPQC particles, specifically PoPQC10:1, maintained a relatively constant size at 100–250 mM NaCl, indicating that QC conjugation limited electrostatic screening of the protein molecules.

The pH influenced PoP adsorption and interfacial film formation at the O/W interface. A moderate viscoelastic film network was formed resulting from the repulsive force of PoP molecules at pH far away from pI. The complexation of PoP with QC limited the protein aggregation, particularly for pH 5.0, where the hydrophobic regions of PoP were potentially masked by QC, hindering the hydrophobic attraction among protein molecules and promoting the formation of an elastic interfacial layer evidenced by interfacial shear rheology. Protein aggregation was caused by [NaCl] shielding the surface charge of PoP, which slightly affected their interaction and adsorption at interface. Nonetheless, ion screening of the protein was reduced owing to PoP complexed with QC, resulting in a slight improvement of the adsorption behavior of PoPQC at the interface. These properties, ultimately resulted in enhanced gastric stability such that PoPQC-stabilized Pickering

emulsions largely maintained droplet integrity whilst PoP-stabilised emulsions demonstrated droplet coalescence. This was attributed to the robustness of hybrid interfacial layers of PoPQC restricting the proteolysis during gastric digestion as well as providing the stability of hybrid particles at the interface. These results demonstrated that tailoring hybrid PoPQC particles is an effective approach to controlling interfacial film behaviors in various environmental conditions, and enable gastric stability, making hybrid PoPQC particles a promising plant-based Pickering stabilizer for controlled delivery applications.

Acknowledgements

This work was funded by the UK National Alternative Protein Innovation Centre (NAPIC), which is an Innovation and Knowledge Centre funded by the Biotechnology and Biological Sciences Research Council (BBSRC) and Innovate UK (Grant Ref: BB/Z516119/1). Author NN acknowledges research financial support from the Rajamangala University of Technology Krungthep (RMUTK), Thailand, for a PhD academic scholarship. Authors thank Dr. Ruth Hughes from Faculty of Biological Sciences at the University of Leeds for their technical support for CLSM imaging.

References

Akgonullu, D. Z., O'Hagan, N. M., Murray, B. S., Connell, S. D., Fang, Y., Linter, B. R., & Sarkar, A. (2024). Bulk and Interfacial Behavior of Potato Protein-Based Microgels. *Langmuir, 40*(41), 21341-21351. https://doi.org/https://doi.org/10.1021/acs.langmuir.4c01785.

Alghamdi, A., Birch, D. J. S., Vyshemirsky, V., & Rolinski, O. J. (2022). Impact of the Flavonoid Quercetin on β-Amyloid Aggregation Revealed by Intrinsic Fluorescence. *The Journal of Physical Chemistry B, 126*(38), 7229-7237. https://doi.org/https://doi.org/10.1021/acs.jpcb.2c02763.

Andlinger, D. J., Röscheisen, P., Hengst, C., & Kulozik, U. (2021). Influence of pH, Temperature and Protease Inhibitors on Kinetics and Mechanism of Thermally Induced Aggregation of Potato Proteins. *10*(4), 796. https://www.mdpi.com/2304-8158/10/4/796.

Araiza-Calahorra, A., Glover, Z. J., Akhtar, M., & Sarkar, A. (2020). Conjugate microgel-stabilized Pickering emulsions: Role in delaying gastric digestion. *Food Hydrocolloids, 105*, 105794. https://doi.org/https://doi.org/10.1016/j.foodhyd.2020.105794.

Araiza-Calahorra, A., & Sarkar, A. (2019). Designing biopolymer-coated Pickering emulsions to modulate in vitro gastric digestion: a static model study. *Food & Function, 10*(9), 5498-5509. https://doi.org/https://doi.org/10.1039/C9FO01080G.

Bergfreund, J., Bertsch, P., & Fischer, P. (2021a). Adsorption of proteins to fluid interfaces: Role of the hydrophobic subphase. *Journal of Colloid and Interface Science, 584*, 411-417. https://doi.org/https://doi.org/10.1016/j.jcis.2020.09.118.

Bergfreund, J., Diener, M., Geue, T., Nussbaum, N., Kummer, N., Bertsch, P., . . . Fischer, P. (2021b). Globular protein assembly and network formation at fluid interfaces: effect of oil. *Soft Matter, 17*(6), 1692-1700. https://doi.org/http://dx.doi.org/10.1039/D0SM01870H.

Bertsch, P., & Fischer, P. (2019). Interfacial Rheology of Charged Anisotropic Cellulose Nanocrystals at the Air–Water Interface. *Langmuir, 35*(24), 7937-7943. https://doi.org/https://doi.org/10.1021/acs.langmuir.9b00699.

Bevan, M., Barker, R., Goldsbrough, A., Jarvis, M., Kavanagh, T., & Iturriaga, G. (1986). The structure and transcription start site of major potato tuber protine gene. *Nucleic Acids Research, 14*(11), 4625-4638. https://doi.org/https://doi.org/10.1093/nar/14.11.4625.

Bock, A., Kieserling, H., Rohn, S., Steinhäuser, U., & Drusch, S. (2022). Impact of Phenolic Acid Derivatives on β-Lactoglobulin Stabilized Oil-Water-Interfaces. *Food Biophysics, 17*(4), 508-522. https://doi.org/https://doi.org/10.1007/s11483-022-09737-8.

Cai, Z., Wei, Y., Shi, A., Zhong, J., Rao, P., Wang, Q., & Zhang, H. (2023). Correlation between interfacial layer properties and physical stability of food emulsions: current trends, challenges, strategies, and further perspectives. *Advances in Colloid and Interface Science, 313*, 102863. https://doi.org/https://doi.org/10.1016/j.cis.2023.102863.

Cao, Y., Wang, Q., & Xiong, Y. L. (2025). Differential binding of gallic acid and epigallocatechin gallate to whey protein affects the interfacial adsorption and gastric digestion of O/W emulsion. *Food Chemistry, 464*, 141672. https://doi.org/https://doi.org/10.1016/j.foodchem.2024.141672.

Chen, Y., Yi, X., Zhang, Z., Ding, B., Li, Z., & Luo, Y. (2022). High internal phase Pickering emulsions stabilized by tannic acid-ovalbumin complexes: Interfacial property and stability. *Food Hydrocolloids, 125*, 107332. https://doi.org/https://doi.org/10.1016/j.foodhyd.2021.107332.

Cheng, J., Dudu, O. E., Zhang, J., Wang, Y., Meng, L., Wei, W., . . . Yan, T. (2023). Impact of binding interaction modes between whey protein concentrate and quercetin on protein structural and functional characteristics. *Food Hydrocolloids, 142*, 108787. https://doi.org/https://doi.org/10.1016/j.foodhyd.2023.108787.

Dai, L., Zhan, X., Wei, Y., Sun, C., Mao, L., McClements, D. J., & Gao, Y. (2018). Composite zein - propylene glycol alginate particles prepared using solvent evaporation: Characterization and application as Pickering emulsion stabilizers. *Food Hydrocolloids, 85*, 281-290. https://doi.org/https://doi.org/10.1016/j.foodhyd.2018.07.013.

Dai, T., Li, T., Li, R., Zhou, H., Liu, C., Chen, J., & McClements, D. J. (2020). Utilization of plant-based protein-polyphenol complexes to form and stabilize emulsions: Pea proteins and grape seed proanthocyanidins. *Food Chemistry, 329*, 127219. https://doi.org/https://doi.org/10.1016/j.foodchem.2020.127219.

Dickinson, E. (1998). Proteins at interfaces and in emulsions Stability, rheology and interactions. *Journal of the Chemical Society, Faraday Transactions, 94*(12), 1657-1669. https://doi.org/https://doi.org/10.1039/A801167B.

Dickinson, E. (1999). Adsorbed protein layers at fluid interfaces: interactions, structure and surface rheology. *Colloids and Surfaces B: Biointerfaces, 15*(2), 161-176. https://doi.org/https://doi.org/10.1016/S0927-7765(99)00042-9.

Du, C.-X., Xu, J.-J., Luo, S.-Z., Li, X.-J., Mu, D.-D., Jiang, S.-T., & Zheng, Z. (2022). Low-oil-phase emulsion gel with antioxidant properties prepared by soybean protein isolate and curcumin composite nanoparticles. *LWT, 161*, 113346. https://doi.org/https://doi.org/10.1016/j.lwt.2022.113346.

Eichhorn, M., Thorenz, E., & Drusch, S. (2025). Behaviour of potato protein-pectin conjugates in emulsions: insights from interfacial shear rheology. *Food Hydrocolloids*, 111107. https://doi.org/https://doi.org/10.1016/j.foodhyd.2025.111107.

Felix, M., Romero, A., Carrera-Sanchez, C., & Guerrero, A. (2019). Assessment of interfacial viscoelastic properties of Faba bean (Vicia faba) protein-adsorbed O/W layers as a function of pH. *Food Hydrocolloids, 90*, 353-359. https://doi.org/https://doi.org/10.1016/j.foodhyd.2018.12.036.

Feng, T., Wang, X., Wang, X., Xia, S., & Huang, Q. (2021). Plant protein-based antioxidant Pickering emulsions and high internal phase Pickering emulsions against broad pH range and high ionic strength: Effects of interfacial rheology and microstructure. *LWT, 150*, 111953. https://doi.org/https://doi.org/10.1016/j.lwt.2021.111953.

Guha, S., Majumder, K., & Mine, Y. (2019). Egg Proteins. In L. Melton, F. Shahidi & P. Varelis (Eds.), *Encyclopedia of Food Chemistry* (pp. 74-84). Oxford: Academic Press.

Gul, O., Gul, L. B., Baskıncı, T., Parlak, M. E., & Saricaoglu, F. T. (2023). Influence of pH and ionic strength on the bulk and interfacial rheology and technofunctional properties of hazelnut meal protein isolate. *Food Research International, 169*, 112906. https://doi.org/https://doi.org/10.1016/j.foodres.2023.112906.

Han, S., Cui, F., McClements, D. J., Xu, X., Ma, C., Wang, Y., . . . Liu, F. (2022). Structural Characterization and Evaluation of Interfacial Properties of Pea Protein Isolate-EGCG Molecular Complexes. *Foods, 11*(18), 2895. https://doi.org/https://doi.org/10.3390/foods11182895.

Hashemi-Shahraki, F., Shareghi, B., & Farhadian, S. (2023). Investigation of the interaction behavior between quercetin and pepsin by spectroscopy and MD simulation methods. *International Journal of Biological Macromolecules, 227*, 1151-1161. https://doi.org/https://doi.org/10.1016/j.ijbiomac.2022.11.296.

Hinderink, E. B. A., Sagis, L., Schroën, K., & Berton-Carabin, C. C. (2021). Sequential adsorption and interfacial displacement in emulsions stabilized with plant-dairy protein blends. *Journal of Colloid and Interface Science, 583*, 704-713. https://doi.org/https://doi.org/10.1016/j.jcis.2020.09.066.

Hu, C., & Xiong, H. (2022). Structure, interfacial adsorption and emulsifying properties of potato protein isolate modified by chitosan. *Colloids and Surfaces A: Physicochemical and Engineering Aspects, 638*, 128314. https://doi.org/https://doi.org/10.1016/j.colsurfa.2022.128314.

Ikenaga, N., & Sagis, L. M. C. (2024). Interfacial moduli at large strains and stability of emulsions stabilised by plant proteins at high bulk shear rates. *Food Hydrocolloids, 146*, 109248. https://doi.org/https://doi.org/10.1016/j.foodhyd.2023.109248.

Ju, M., Zhu, G., Huang, G., Shen, X., Zhang, Y., Jiang, L., & Sui, X. (2020). A novel pickering emulsion produced using soy protein-anthocyanin complex nanoparticles. *Food Hydrocolloids, 99*, 105329. https://doi.org/https://doi.org/10.1016/j.foodhyd.2019.105329.

Kew, B., Holmes, M., Stieger, M., & Sarkar, A. (2021). Oral tribology, adsorption and rheology of alternative food proteins. *Food Hydrocolloids, 116*, 106636. https://doi.org/https://doi.org/10.1016/j.foodhyd.2021.106636.

Kieserling, H., Pankow, A., Keppler, J. K., Wagemans, A. M., & Drusch, S. (2021). Conformational state and charge determine the interfacial film formation and film stability of β-lactoglobulin. *Food Hydrocolloids, 114*, 106561. https://doi.org/https://doi.org/10.1016/j.foodhyd.2020.106561.

Lavoisier, A., Vilgis, T. A., & Aguilera, J. M. (2019). Effect of cysteine addition and heat treatment on the properties and microstructure of a calcium-induced whey protein cold-set gel. *Current Research in Food Science, 1*, 31-42. https://doi.org/https://doi.org/10.1016/j.crfs.2019.10.001.

Li, J., Ye, A., Lee, S. J., & Singh, H. (2012). Influence of gastric digestive reaction on subsequent in vitro intestinal digestion of sodium caseinate-stabilized emulsions. *Food & Function, 3*(3), 320-326. https://doi.org/https://doi.org/10.1039/C2FO10242K.

Li, R., Dai, T., Tan, Y., Fu, G., Wan, Y., Liu, C., & McClements, D. J. (2020). Fabrication of pea protein-tannic acid complexes: Impact on formation, stability, and digestion of flaxseed oil emulsions. *Food Chemistry, 310*, 125828. https://doi.org/https://doi.org/10.1016/j.foodchem.2019.125828.

Liu, Y., Liu, C., Zhang, S., Li, J., Zheng, H., Jin, H., & Xu, J. (2021). Comparison of Different Protein Emulsifiers on Physicochemical Properties of β-Carotene-Loaded Nanoemulsion: Effect on Formation, Stability, and In Vitro Digestion. *Nanomaterials, 11*(1), 167. https://doi.org/https://doi.org/10.3390/nano11010167.

Luo, Z., Murray, B. S., Ross, A.-L., Povey, M. J. W., Morgan, M. R. A., & Day, A. J. (2012). Effects of pH on the ability of flavonoids to act as Pickering emulsion stabilizers. *Colloids and Surfaces B: Biointerfaces, 92*, 84-90. https://doi.org/https://doi.org/10.1016/j.colsurfb.2011.11.027.

Luo, Z., Murray, B. S., Yusoff, A., Morgan, M. R. A., Povey, M. J. W., & Day, A. J. (2011). Particle-Stabilizing Effects of Flavonoids at the Oil−Water Interface. *Journal of Agricultural and Food Chemistry, 59*(6), 2636-2645. https://doi.org/https://doi.org/10.1021/jf1041855.

Maldonado-Valderrama, J., Terriza, J. A. H., Torcello-Gómez, A., & Cabrerizo-Vílchez, M. A. (2013). In vitro digestion of interfacial protein structures. *Soft Matter, 9*(4), 1043-1053. https://doi.org/https://doi.org/10.1039/C2SM26843D.

Minekus, M., Alminger, M., Alvito, P., Ballance, S., Bohn, T., Bourlieu, C., . . . Brodkorb, A. (2014). A standardised static in vitro digestion method suitable for food – an international consensus. *Food & Function, 5*(6), 1113-1124. https://doi.org/http://dx.doi.org/10.1039/C3FO60702J.

Miquelim, J. N., Lannes, S. C. S., & Mezzenga, R. (2010). pH Influence on the stability of foams with protein–polysaccharide complexes at their interfaces. *Food Hydrocolloids, 24*(4), 398-405. https://doi.org/https://doi.org/10.1016/j.foodhyd.2009.11.006.

Murray, B. S. (2002). Interfacial rheology of food emulsifiers and proteins. *Current Opinion in Colloid & Interface Science, 7*(5), 426-431. https://doi.org/https://doi.org/10.1016/S1359-0294(02)00077-8.
Murray, B. S. (2011). Rheological properties of protein films. *Current Opinion in Colloid & Interface Science, 16*(1), 27-35. https://doi.org/https://doi.org/10.1016/j.cocis.2010.06.005.
Murray, B. S., & Dickinson, E. (1996). Interfacial Rheology and the Dynamic Properties of Adsorbed Films of Food Proteins and Surfactants. *Food Science and Technology International, Tokyo, 2*(3), 131-145. https://doi.org/https://doi.org/10.3136/fsti9596t9798.2.131.
Nayak, A., Genot, C., Meynier, A., Dorlando, A., & Capron, I. (2022). Impact of process and physico-chemical conditions on the formation of curcumin-whey protein composite particles capable to stabilize food-compatible oil in water emulsions. *LWT, 153*, 112421. https://doi.org/https://doi.org/10.1016/j.lwt.2021.112421.
Nimaming, N., Sadeghpour, A., Murray, B. S., & Sarkar, A. (2024). Pickering oil-in-water emulsions stabilized by hybrid plant protein-flavonoid conjugate particles. *Food Hydrocolloids, 154*, 110146. https://doi.org/https://doi.org/10.1016/j.foodhyd.2024.110146.
Ntone, E., van Wesel, T., Sagis, L. M. C., Meinders, M., Bitter, J. H., & Nikiforidis, C. V. (2021). Adsorption of rapeseed proteins at oil/water interfaces. Janus-like napins dominate the interface. *Journal of Colloid and Interface Science, 583*, 459-469. https://doi.org/https://doi.org/10.1016/j.jcis.2020.09.039.
Qin, X.-S., Gao, Q.-Y., & Luo, Z.-G. (2021). Enhancing the storage and gastrointestinal passage viability of probiotic powder (Lactobacillus Plantarum) through encapsulation with pickering high internal phase emulsions stabilized with WPI-EGCG covalent conjugate nanoparticles. *Food Hydrocolloids, 116*, 106658. https://doi.org/https://doi.org/10.1016/j.foodhyd.2021.106658.
Qin, X.-S., Luo, Z.-G., Peng, X.-C., Lu, X.-X., & Zou, Y.-X. (2018). Fabrication and Characterization of Quinoa Protein Nanoparticle-Stabilized Food-Grade Pickering Emulsions with Ultrasound Treatment: Effect of Ionic Strength on the Freeze–Thaw Stability. *Journal of Agricultural and Food Chemistry, 66*(31), 8363-8370. https://doi.org/https://doi.org/10.1021/acs.jafc.8b02407.
Qin, X., Yu, J., Wang, Q., Zhang, H., Chen, H., Hu, Z., . . . Liu, G. (2022). Preparation of camellia oil pickering emulsion stabilized by glycated whey protein isolate and chitooligosaccharide: Effect on interfacial behavior and emulsion stability. *LWT, 153*, 112515. https://doi.org/https://doi.org/10.1016/j.lwt.2021.112515.
Romoscanu, A. I., & Mezzenga, R. (2005). Cross Linking and Rheological Characterization of Adsorbed Protein Layers at the Oil−Water Interface. *Langmuir, 21*(21), 9689-9697. https://doi.org/https://doi.org/10.1021/la051241t.
Rühs, P. A., Scheuble, N., Windhab, E. J., Mezzenga, R., & Fischer, P. (2012). Simultaneous Control of pH and Ionic Strength during Interfacial Rheology of β-Lactoglobulin Fibrils Adsorbed at Liquid/Liquid Interfaces. *Langmuir, 28*(34), 12536-12543. https://doi.org/https://doi.org/10.1021/la3026705.
Sarkar, A., Ademuyiwa, V., Stubley, S., Esa, N. H., Goycoolea, F. M., Qin, X., . . . Olvera, C. (2018). Pickering emulsions co-stabilized by composite protein/ polysaccharide particle-particle interfaces: Impact on in vitro gastric stability. *Food Hydrocolloids, 84*, 282-291. https://doi.org/https://doi.org/10.1016/j.foodhyd.2018.06.019.
Sarkar, A., & Dickinson, E. (2020). Sustainable food-grade Pickering emulsions stabilized by plant-based particles. *Current Opinion in Colloid & Interface Science, 49*, 69-81. https://doi.org/https://doi.org/10.1016/j.cocis.2020.04.004.
Sarkar, A., Goh, K. K. T., Singh, R. P., & Singh, H. (2009). Behaviour of an oil-in-water emulsion stabilized by β-lactoglobulin in an in vitro gastric model. *Food Hydrocolloids, 23*(6), 1563-1569. https://doi.org/https://doi.org/10.1016/j.foodhyd.2008.10.014.
Sarkar, A., & Singh, H. (2016). Emulsions and Foams Stabilised by Milk Proteins. In P. L. H. McSweeney & J. A. O'Mahony (Eds.), *Advanced Dairy Chemistry: Volume 1B: Proteins: Applied Aspects* (pp. 133-153). New York, NY: Springer New York.
Sarkar, A., Zhang, S., Holmes, M., & Ettelaie, R. (2019). Colloidal aspects of digestion of Pickering emulsions: Experiments and theoretical models of lipid digestion kinetics. *Advances in Colloid and Interface Science, 263*, 195-211. https://doi.org/https://doi.org/10.1016/j.cis.2018.10.002.
Scheuble, N., Geue, T., Windhab, E. J., & Fischer, P. (2014). Tailored Interfacial Rheology for Gastric Stable Adsorption Layers. *Biomacromolecules, 15*(8), 3139-3145. https://doi.org/https://doi.org/10.1021/bm500767c.
Shishikura, Y., Khokhar, S., & Murray, B. S. (2006). Effects of Tea Polyphenols on Emulsification of Olive Oil in a Small Intestine Model System. *Journal of Agricultural and Food Chemistry, 54*(5), 1906-1913. https://doi.org/https://doi.org/10.1021/jf051988p.
Singh, H., & Sarkar, A. (2011). Behaviour of protein-stabilised emulsions under various physiological conditions. *Advances in Colloid and Interface Science, 165*(1), 47-57. https://doi.org/https://doi.org/10.1016/j.cis.2011.02.001.
Singh, H., Ye, A., & Ferrua, M. J. (2015). Aspects of food structures in the digestive tract. *Current Opinion in Food Science, 3*, 85-93. https://doi.org/https://doi.org/10.1016/j.cofs.2015.06.007.
Singh, H., Ye, A., & Horne, D. (2009). Structuring food emulsions in the gastrointestinal tract to modify lipid digestion. *Progress in Lipid Research, 48*(2), 92-100. https://doi.org/https://doi.org/10.1016/j.plipres.2008.12.001.

Su, J., Guo, Q., Chen, Y., Mao, L., Gao, Y., & Yuan, F. (2020). Utilization of β-lactoglobulin- (−)-Epigallocatechin- 3-gallate(EGCG) composite colloidal nanoparticles as stabilizers for lutein pickering emulsion. *Food Hydrocolloids, 98*, 105293. https://doi.org/https://doi.org/10.1016/j.foodhyd.2019.105293.

Yang, M., Zhi, Y., W., E. D., Paul, G. E., Harjinder, S., & and Ye, A. (2025). Digestion of food proteins: the role of pepsin. *Critical Reviews in Food Science and Nutrition*, 1-22. https://doi.org/10.1080/10408398.2025.2453096.

Yin, L., Cao, Y., Wang, M., Kong, B., Liu, Q., Wang, H., & Wang, H. (2025). Zein-quercetin covalent nanoparticles encapsulating oregano essential oil: Improved stability, antioxidant, and antibacterial properties. *Process Biochemistry, 149*, 248-259. https://doi.org/https://doi.org/10.1016/j.procbio.2024.12.015.

Zaplatic, E., Bule, M., Shah, S. Z. A., Uddin, M. S., & Niaz, K. (2019). Molecular mechanisms underlying protective role of quercetin in attenuating Alzheimer's disease. *Life Sciences, 224*, 109-119. https://doi.org/https://doi.org/10.1016/j.lfs.2019.03.055.

Zembyla, M., Lazidis, A., Murray, B. S., & Sarkar, A. (2020). Stability of water-in-oil emulsions co-stabilized by polyphenol crystal-protein complexes as a function of shear rate and temperature. *Journal of Food Engineering, 281*, 109991. https://doi.org/https://doi.org/10.1016/j.jfoodeng.2020.109991.

Zembyla, M., Murray, B. S., Radford, S. J., & Sarkar, A. (2019). Water-in-oil Pickering emulsions stabilized by an interfacial complex of water-insoluble polyphenol crystals and protein. *Journal of Colloid and Interface Science, 548*, 88-99. https://doi.org/https://doi.org/10.1016/j.jcis.2019.04.010.

Zembyla, M., Murray, B. S., & Sarkar, A. (2018). Water-In-Oil Pickering Emulsions Stabilized by Water-Insoluble Polyphenol Crystals. *Langmuir, 34*(34), 10001-10011. https://doi.org/https://doi.org/10.1021/acs.langmuir.8b01438.

Zhang, S., Murray, B. S., Suriyachay, N., Holmes, M., Ettelaie, R., & Sarkar, A. (2021a). Synergistic Interactions of Plant Protein Microgels and Cellulose Nanocrystals at the Interface and Their Inhibition of the Gastric Digestion of Pickering Emulsions. *Langmuir, 37*(2), 827-840. https://doi.org/https://doi.org/10.1021/acs.langmuir.0c03148.

Zhang, X., Lei, Y., Luo, X., Wang, Y., Li, Y., Li, B., & Liu, S. (2021b). Impact of pH on the interaction between soybean protein isolate and oxidized bacterial cellulose at oil-water interface: Dilatational rheological and emulsifying properties. *Food Hydrocolloids, 115*, 106609. https://doi.org/https://doi.org/10.1016/j.foodhyd.2021.106609.

Zhao, J., Wang, S., Jiang, D., Chen, C., Tang, J., Tomasevic, I., & Sun, W. (2023). The influence of protein oxidation on structure, pepsin diffusion, and in vitro gastric digestion of SPI emulsion. *Food Chemistry, 428*, 136791. https://doi.org/https://doi.org/10.1016/j.foodchem.2023.136791.

Zheng, X., Ren, C., Wei, Y., Wang, J., Xu, X., Du, M., & Wu, C. (2023). Soy protein particles with enhanced anti-aggregation behaviors under various heating temperatures, pH, and ionic strengths. *Food Research International, 170*, 112924. https://doi.org/https://doi.org/10.1016/j.foodres.2023.112924.

Zhou, S.-D., Lin, Y.-F., Xu, X., Meng, L., & Dong, M.-S. (2020). Effect of non-covalent and covalent complexation of (−)-epigallocatechin gallate with soybean protein isolate on protein structure and in vitro digestion characteristics. *Food Chemistry, 309*, 125718. https://doi.org/https://doi.org/10.1016/j.foodchem.2019.125718.

Zou, Y., Zhong, J., Pan, R., Wan, Z., Guo, J., Wang, J., . . . Yang, X. (2017). Zein/tannic acid complex nanoparticles-stabilised emulsion as a novel delivery system for controlled release of curcumin. *International Journal of Food Science & Technology, 52*(5), 1221-1228. https://doi.org/https://doi.org/10.1111/ijfs.13380.

Supplementary Information

Interfacial properties of plant protein–flavonoid hybrid particles: Towards influencing *in vitro* gastric digestion of emulsions

Nisufyan Nimaming[1, 2], Amin Sadeghpour[1], Brent S. Murray[1, 3],

Anwesha Sarkar[1, 3]*

[1]*Food Colloids and Bioprocessing Group, School of Food Science and Nutrition, University of Leeds, Leeds, LS2 9JT, United Kingdom.*

[2]*Food and Nutrition, Faculty of Home Economics Technology, Rajamangala University of Technology Krungthep, Bangkok, 10120, Thailand*

[3]*National Alternative Protein Innovation Centre (NAPIC), UK*

Corresponding authors:

*Prof. Anwesha Sarkar

[1] Food Colloids and Bioprocessing Group, School of Food Science and Nutrition, University of Leeds, Leeds LS2 9JT, UK.

[3] National Alternative Protein Innovation Centre (NAPIC), UK

E-mail address: A.Sarkar@leeds.ac.uk

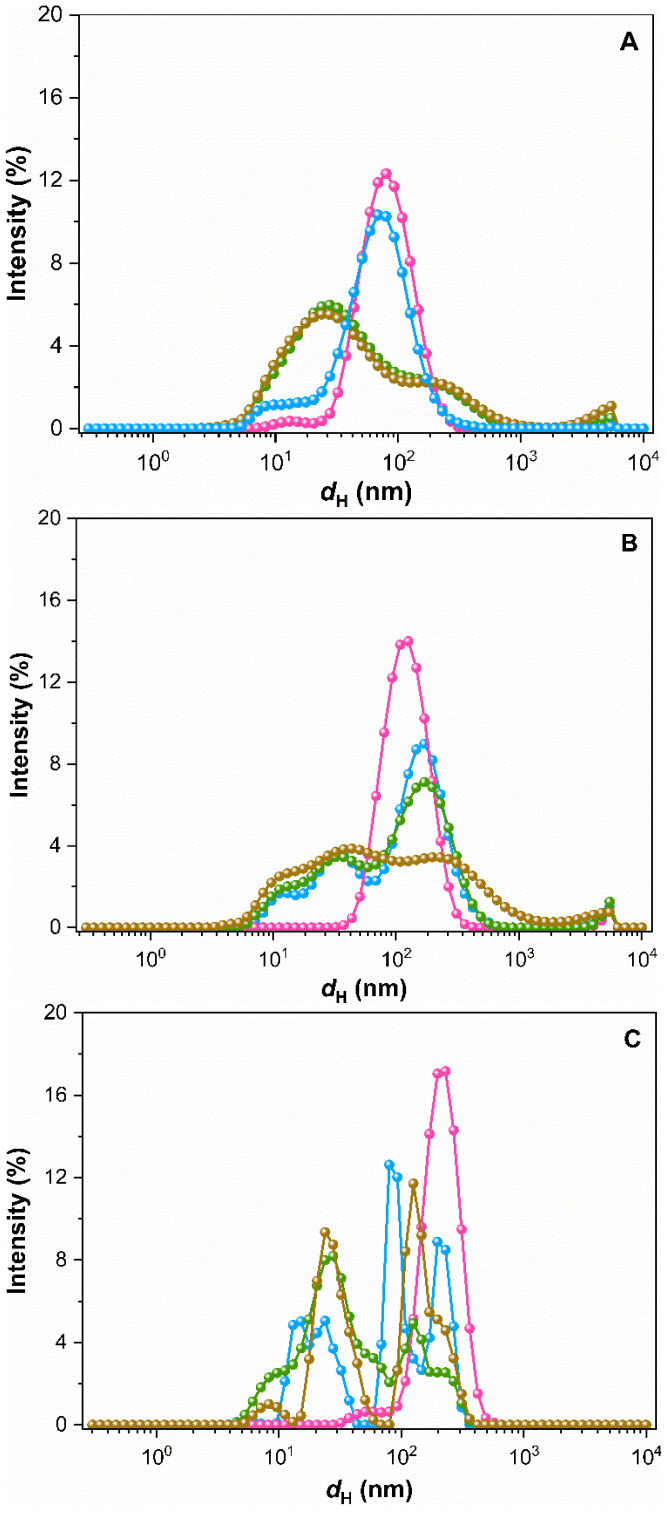

Fig. S1. Mean particle size distribution of PoP (**A**), hybrid PoPQC10:1 (**B**), and PoPQC10:1.5 (**C**) particles as a function of pH (pH 3.0: ●, pH 5.0: ●, pH 7.0: ●, and pH 9.0: ●). The data were reported as an average value of at least three repeats on three independent experiments (n = 3 × 3).

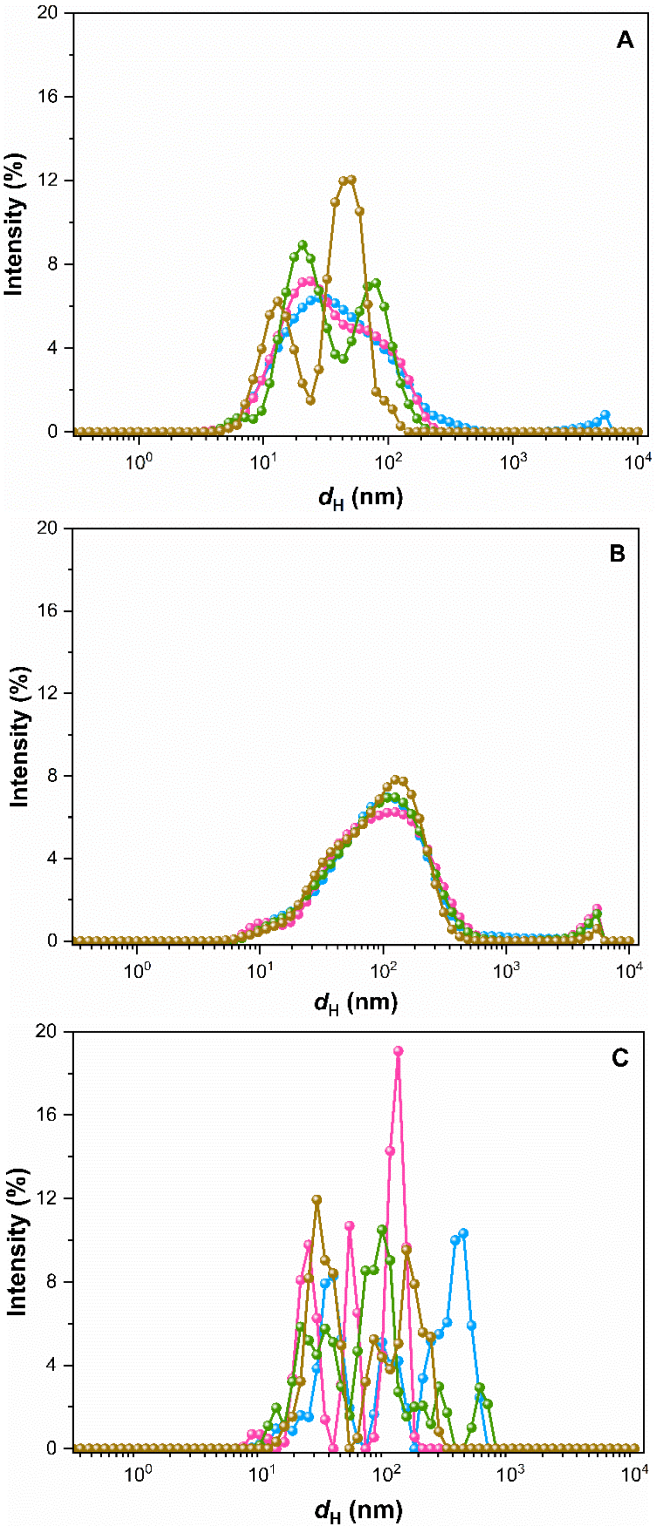

Fig S2. Mean particle size distribution of PoP (**A**), hybrid PoPQC10:1 (**B**), and PoPQC10:1.5 (**C**) particles as a function of ionic strength (100 mM: ●, 150 mM: ●, 200 mM: ●, and 250 mM: ●). The data were reported as an average value of at least three repeats on three independent experiments (n = 3 × 3).

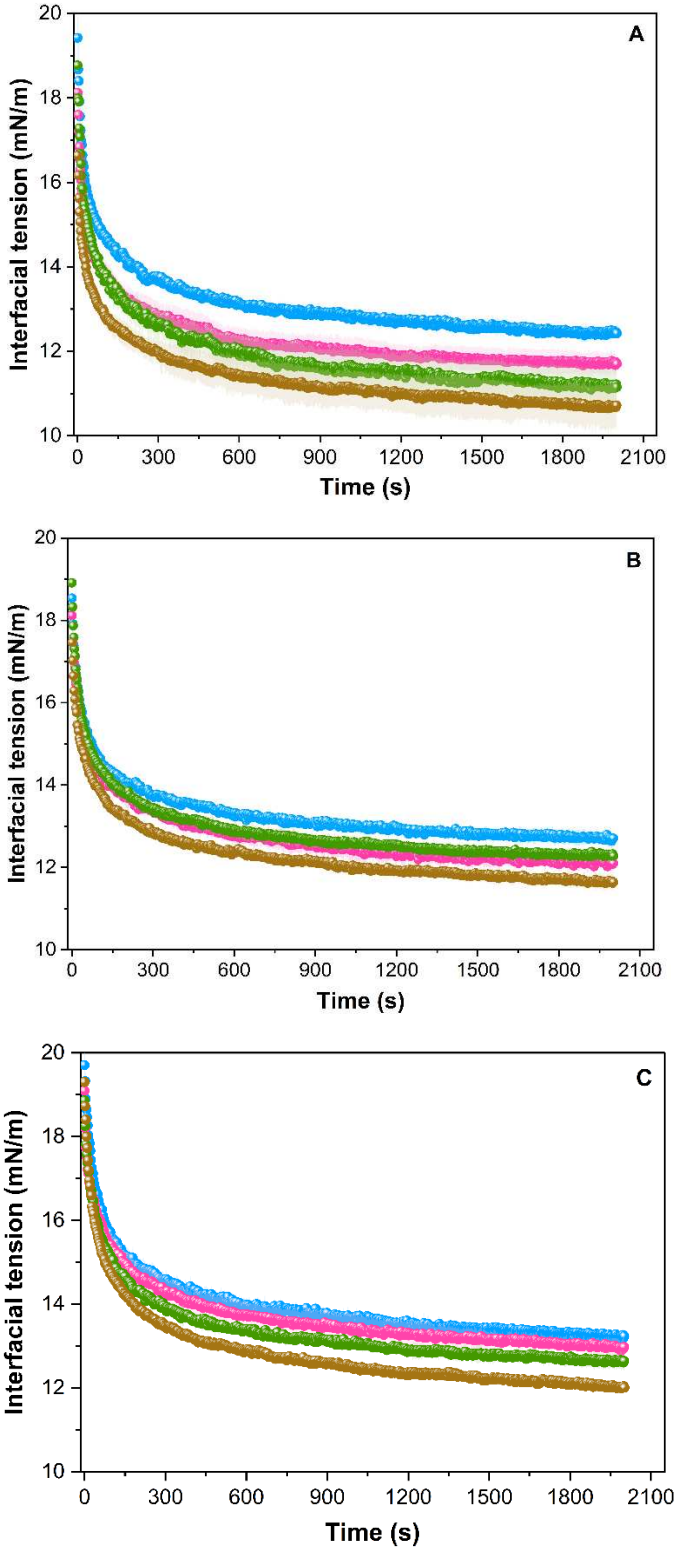

876

877 **Fig. S3**. Dynamic interfacial tension (γ) of PoP (**A**), PoPQC10:1 (**B**), and PoPQC10:1.5 (**C**)
878 as a function of pH (pH 3.0: ●, pH 5.0: ●, pH 7.0: ●, and pH 9.0: ●). The data were reported
879 as an average value of at least three repeats on three independent experiments (n = 3 × 3).

880 **Table S1.** Characteristic dynamic parameters of adsorption of PoP and hybrid PoPQC
881 particles at O-W interface with different pH values.

Sample	pH	γ_{2000} (mN/m)	$K_{diff} \pm 0.1$ (mN/m/s$^{1/2}$)	$K_{ads} \times 10^{-3}$ (s)	$K_{rear} \times 10^{-3}$ (s)
PoP	3.0	12.4 ± 0.2^{a}	0.6^{a}	1.9 ± 0.4^{ns}	4.6 ± 0.2^{b}
	5.0	11.8 ± 0.1^{b}	0.5^{a}	2.0 ± 0.3^{ns}	3.7 ± 0.6^{b}
	7.0	11.1 ± 0.4^{bc}	0.6^{a}	1.8 ± 0.3^{ns}	4.1 ± 0.9^{b}
	9.0	10.7 ± 0.5^{c}	0.4^{b}	1.7 ± 0.1^{ns}	6.8 ± 1.3^{a}
PoPQC10: 1	3.0	12.7 ± 0.1^{a}	0.4^{b}	1.9 ± 0.4^{ns}	3.8 ± 1.6^{ns}
	5.0	12.1 ± 0.1^{b}	0.4^{b}	2.0 ±0.4^{ns}	4.1± 0.5^{ns}
	7.0	12.2 ± 0.1^{b}	0.5^{a}	2.1 ± 0.7^{ns}	3.1± 1.6^{ns}
	9.0	11.6 ± 0.2^{c}	0.3^{b}	1.7 ± 0.2^{ns}	4.6± 1.1^{ns}
PoPQC10: 1.5	3.0	13.2 ± 0.3^{a}	0.4^{b}	1.8 ± 0.2^{ns}	6.7 ± 0.2^{ns}
	5.0	12.9 ± 0.2^{a}	0.3^{c}	1.6 ± 0.3^{ns}	4.9 ± 1.8^{ns}
	7.0	12.6 ± 0.2^{a}	0.4^{b}	1.7 ± 0.4^{ns}	6.3 ± 1.2^{ns}
	9.0	12.1 ± 0.1^{b}	0.5^{a}	1.6 ± 0.2^{ns}	4.8 ± 1.4^{ns}

882 Mean values with different lowercase letters $^{(a\text{-}c)}$ with the same column for the same sample
883 indicate significant differences ($p < 0.05$), ^{ns} indicates mean values are non-significant
884 differences ($p \geq 0.05$) based on Duncan's multiple range test.

885 **Table S2.** Characteristic rheological parameters of PoP and hybrid PoPQC particles at O-
886 W interface with different pH values.

Sample	pH	G_i' (mPa m) after 960 min	Critical strain (± 0.1 %) after 960 min
PoP	3.0	89 ± 1[a]	3.2[a]
	5.0	96 ± 10[a]	2.2[b]
	7.0	56 ± 1[b]	2.2[b]
	9.0	30 ± 1[c]	3.2[a]
PoPQC10: 1	3.0	164 ± 2[a]	1.5[c]
	5.0	180 ± 16[a]	1.5[c]
	7.0	42 ± 3[b]	2.2[b]
	9.0	25 ± 1[b]	3.2[a]
PoPQC10: 1.5	3.0	80 ± 6[b]	2.2[a]
	5.0	131 ± 2[a]	1.4[b]
	7.0	46 ± 1[c]	1.4[b]
	9.0	28 ± 2[d]	2.2[a]

887 Mean values with different lowercase letters [(a-d)] with the same column for the same sample
888 indicate significant differences ($p < 0.05$) based on Duncan's multiple range test.
889

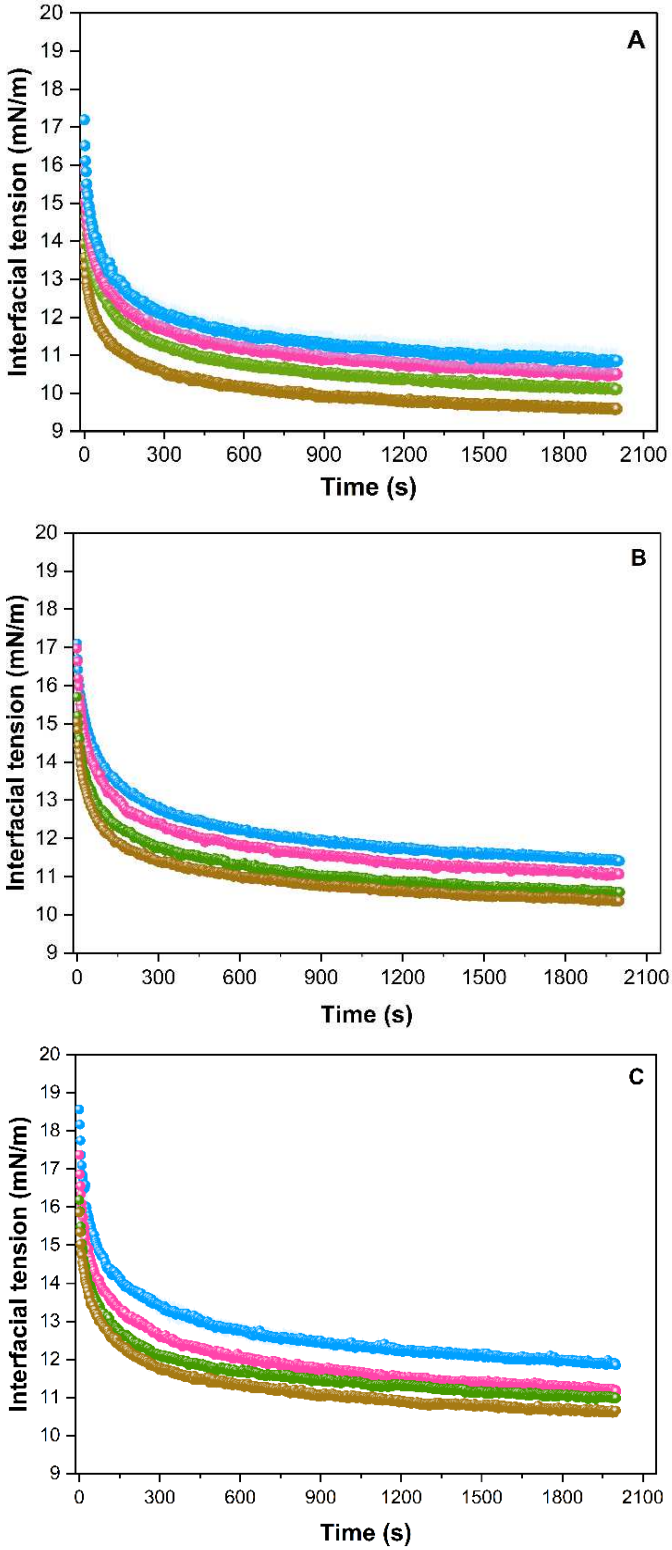

Fig. S4. Dynamic interfacial tension (γ) of PoP (**A**), hybrid PoPQC10:1 (**B**), and PoPQC10:1.5 (**C**) particles as a function of ionic strength (100 mM: ●, 150 mM: ●, 200 mM: ●, and 250 mM: ●). The data were reported as an average value of at least three repeats on three independent experiments (n = 3 × 3).

Table S3. Dynamic adsorption parameters of PoP and hybrid PoPQC particles (pH 7.0) at O-W interface with different concentrations of NaCl [NaCl].

Sample	[NaCl] (mM)	γ_{2000} (mN/m)	$K_{diff} \pm 0.1$ (mN/m/s$^{1/2}$)	$K_{ads} \times 10^{-3}$ (s)	$K_{rear} \times 10^{-3}$ (s)
PoP	100	10.9 ± 0.4^{a}	0.4^{a}	1.9 ± 0.2^{ns}	6.3 ± 1.7^{ab}
	150	10.5 ± 0.1^{a}	0.3^{b}	1.6 ± 0.2^{ns}	7.6 ± 1.6^{a}
	200	10.1 ± 0.1^{b}	0.3^{b}	1.7 ± 0.2^{ns}	3.9 ± 0.7^{b}
	250	10.0 ± 0.1^{c}	0.3^{b}	1.7 ± 0.2^{ns}	4.3 ± 1.8^{b}
PoPQC10: 1	100	11.4 ± 0.1^{a}	0.3^{ab}	1.8 ± 0.4^{ns}	3.6 ± 1.3^{ns}
	150	11.1 ± 0.1^{b}	0.3^{a}	1.8 ± 0.4^{ns}	3.4 ± 1.3^{ns}
	200	10.6 ± 0.1^{c}	0.3^{b}	1.7 ± 0.2^{ns}	4.2 ± 1.7^{ns}
	250	10.4 ± 0.1^{d}	0.3^{b}	1.7 ± 0.1^{ns}	5.4 ± 1.4^{ns}
PoPQC10: 1.5	100	11.8 ± 0.1^{a}	0.4^{a}	1.6 ± 0.1^{ns}	3.3 ± 1.1^{ns}
	150	11.7 ± 0.1^{b}	0.3^{b}	1.7 ± 0.1^{ns}	4.3 ± 1.7^{ns}
	200	10.9 ± 0.1^{c}	0.3^{c}	1.5 ± 0.2^{ns}	5.9 ± 1.6^{ns}
	250	10.6 ± 0.1^{d}	0.3^{bc}	1.8 ± 0.3^{ns}	4.6 ± 0.8^{ns}

Mean values with different lowercase letters $^{(a\text{-}d)}$ with the same column for the same sample indicate significant differences ($p < 0.05$), ^{ns} indicates mean values are non-significant differences ($p \geq 0.05$) based on Duncan's multiple range test.

Table S4. Characteristic rheological parameters of PoP and hybrid PoPQC particles (pH 7.0) at O-W interface with different with different concentrations of NaCl [NaCl].

Sample	[NaCl] (mM)	G_i' (mPa m) after 960 min	critical strain (± 0.1 %) after 960 min
PoP	0	56 ± 1^{a}	2.2^{a}
	100	42 ± 7^{b}	1.5^{b}
	150	45 ± 1^{ab}	1.5^{b}
	200	47 ± 5^{ab}	2.2^{a}
	250	44 ± 4^{ab}	2.2^{a}
PoPQC10: 1	0	42 ± 3^{b}	2.2^{ns}
	100	33 ± 4^{c}	2.2^{ns}
	150	64 ± 4^{a}	2.2^{ns}
	200	50 ± 4^{b}	2.2^{ns}
	250	47 ± 2^{b}	2.2^{ns}
PoPQC10: 1.5	0	46 ± 1^{c}	1.4^{b}
	100	45 ± 8^{bc}	2.2^{a}
	150	51 ± 1^{bc}	2.2^{a}
	200	74 ± 2^{a}	2.2^{a}
	250	54 ± 3^{b}	2.2^{a}

Mean values with different lowercase letters $^{(a\text{-}c)}$ with the same column for the same sample indicate significant differences ($p < 0.05$), ^{ns} indicates mean values are non-significant differences ($p \geq 0.05$) based on Duncan's multiple range test.